Molecular Ion Spectroscopy: New Methods and the Proposed Study of H_2CO^+

Michael W. Porambo

Prospectus for Preliminary Examination

Department of Chemistry, School of Chemical Sciences

University of Illinois

December 15, 2011

171 RAL

9:00 AM

Motivation and Background

Gas-phase molecular ions inspire much interest in many areas of chemical research, such as combustion and atmospheric processes, and they are thought to play a very important role in the chemistry of the interstellar medium (ISM). Not only can they be probes of interstellar physical conditions, but they also are thought to drive the gas-phase chemistry of the ISM, where the low temperatures preclude reactions with high activation energies. Thus, studying reactions and physical properties of molecular ions confirmed or conjectured to be in the ISM can greatly enhance understanding of the physics and chemistry of interstellar space.

The predominant tool to observe molecular ion chemistry in the ISM is spectroscopy. In order to interpret complicated spectra obtained from observational instruments, experimental spectra of candidate and confirmed species are necessary. Precise spectral information such as transition frequencies, rotational constants, and line strengths obtained from laboratory experiments can be used by observers to streamline searches for candidate species and more precisely determine properties of the environment in which they occur. Several techniques have been developed in the last few decades to selectively perform spectroscopy on molecular ions. For example, velocity modulation spectroscopy (VMS) [1] uses an AC plasma to sinusoidally Doppler-shift the absorption frequency of molecular ions, allowing an ionic absorption signal to be detected at the modulation frequency. In addition, direct absorption on a fast ion beam was accomplished two decades ago for a small number of simple molecular ions [2–4]. Recently, the McCall group has increased the sensitivity of VMS by placing the plasma in an optical cavity [5,6]. A primary goal of our research group is to obtain precise, high resolution spectra of astronomically relevant molecular ions to aid in their detection in the ISM, as well as to further understanding of their fundamental physical and chemical properties. To this end, I have been involved in projects developing a highly sensitive and precise spectroscopic technique for application on a positive column discharge setup and an ion beam instrument.

Previous and Current Work

Positive Column Discharge Spectroscopy

Difficulty in producing a high abundance of ions can present a major challenge to ion spectroscopy. In specialized ion production methods that result in low ion number densities, it becomes crucial to have a highly sensitive spectroscopic technique. To achieve this sensitivity, we have developed a new technique that combines the previous cavity enhanced velocity modulation spectroscopy (CEVMS) [5, 6] method with a noise immune cavity enhanced optical heterodyne molecular spectroscopy (NICE-OHMS) system [7, 8]. We call this technique noise immune cavity enhanced optical heterodyne velocity modulation spectroscopy (NICE-OHVMS) [9]. To fully characterize and optimize this method, we used the $A^2\Pi_u - X^2\Sigma_g^+$ 1–0 Meinel band of N_2^+ as a test system, probing the rovibronic transitions in the near infrared with a commercial tunable titanium-sapphire laser. The N_2^+ ions were produced in the positive column of a glow discharge plasma struck between two electrodes powered by a 4 kV_{pp} AC voltage. The glow discharge is advantageous in that it produces a relatively high number density of ions, facilitating acquisition of a strong signal for further optimization.

A basic diagram of the NICE-OHVMS setup is shown in Fig. 1. The laser, with center frequency ν_c, is phase modulated (at frequency ν_{fm}) by an electro-optic modulator (EOM), generating two sideband laser modes (with frequencies $\nu_c + \nu_{fm}$ and $\nu_c - \nu_{fm}$). Thus, there are three laser modes that probe the sample. In this heterodyne scheme, the sum of the beat signals between each sideband and the carrier is detected at ν_{fm}. When all three laser modes are unabsorbed, the two beat signals are equal in magnitude and opposite in phase, resulting in no net signal. As the laser is scanned in frequency space over an absorption profile, the two sidebands are attenuated unequally, such that the net signal is nonzero. Because this scheme is a zero-background technique and encodes the absorption signal at a high frequency which is less affected by $1/f$ noise, the detection noise is diminished relative to a direct absorption scheme.

Another benefit of this technique is that the net signal additionally detects dispersion

of the phase-modulated laser. Every absorption profile has a corresponding dispersion profile, through which the carrier and sideband modes are phase shifted as the laser is scanned, further resulting in an imbalance in the beat signal [10]. Using a phase sensitive detection setup, the net absorption and dispersion signals are collected simultaneously. Simultaneous detection can be accomplished because the absorption and dispersion signal phases are separated by 90°. Each type of detection—absorption and dispersion—have their own unique lineshapes [10, 11].

While the heterodyne scheme lowers the noise, the absorption/dispersion signal intensity is increased by placing the sample in an optical cavity, which increases the path length. To couple all three modes into the optical cavity, ν_{fm} is set equal to a multiple of the free spectral range (FSR) of the cavity. This action allows a degree of noise immunity; any fluctuation in intensity caused by coupling to the cavity, locking electronics, or frequency instability should occur equally to each mode simultaneously, and thus the net signal will not be affected. The laser and the cavity are actively locked on resonance by using the Pound-Drever-Hall technique [12, 13].

In addition to increasing the signal-to-noise ratio, ion-neutral discrimination is accomplished by using velocity modulation. The plasma is modulated at a frequency ν_{vm}=40 kHz. With the bidirectional optical cavity, the absorption/dispersion signal thus modulates at a frequency of $2\nu_{vm}$. Putting all modulation schemes together, the photodetector output is fully processed by demodulating the absorption/dispersion signal at the laser modulation frequency ν_{fm} in a mixer and then further demodulating the mixer output at $2\nu_{vm}$ in a lock-in amplifier.

Figure 2 shows example NICE-OHVMS spectra obtained from the positive column cell. We examined two regimes: the full Doppler-broadened spectra and the spectra at sub-Doppler resolution. Spectra of Meinel lines at ν_{fm}=1 GHz (9 FSRs) were obtained to examine the signal-to-noise and ion-neutral discrimination of the Doppler-broadened line, while ν_{fm}=113 MHz (1 FSR) was used to obtain spectra for sub-Doppler studies. The third-derivative-like lineshape is the result of the demodulations of the signal at ν_{fm} and $2\nu_{vm}$. Lamb dips were observed at multiples of $\nu_{fm}/2$, resulting from a mode of the

forward-propagating beam and a mode from the counter-propagating beam interacting with the same velocity population of ions. The sub-Doppler spectra were obtained for both absorption and dispersion. A sub-Doppler fit equation consisting of Gaussian absorption and corresponding dispersion lineshape functions, based on NICE-OHMS lineshape analysis [10], was applied to the data. By calibrating the spectra with an optical frequency comb [5] and then applying the fit equations, very accurate line centers for the transition could be determined from the sub-Doppler spectra. For example, the $Q_{22}(13)$ transition line center was determined to be 326,187,572.2 MHz with an uncertainty of 300 kHz.

Ion Beam Spectroscopy

Performing spectroscopy on a fast beam of ions has many advantages over other techniques. Ion beam spectra have relatively narrow linewidths due to the phenomenon of kinematic compression, the ion beam itself can be easily integrated with a highly sensitive spectroscopic technique, on-line mass spectrometry can be used to characterize the ion beam, and the ions can be produced in a rotationally cool state with a supersonic expansion source. One of the biggest disadvantages is that a very low ion density ($\sim 10^6$ cm^{-3}) is probed; thus, our new spectroscopic techniques were developed on a positive column source before being used on the ion beam instrument. When completed, this instrument will be known as the Sensitive, Cooled, Resolved Ion BEam Spectrometer (SCRIBES).

A simplified diagram of the ion beam instrument is shown in Fig. 3. The major parts of the ion beam setup are as follows. Ions are produced in a simple cold cathode glow discharge source under vacuum, extracted, and then steered and focused into a collimated ion beam using electrostatic optics and lenses. The ion beam is then turned 90° by a custom cylindrical electrostatic deflector; this element turns the beam into an overlap region to be probed by the laser and separates the charged ions from any residual neutrals that flow from the source. The laser enters and exits the instrument through the optical cavity mirrors, which are separate from the vacuum setup, and windows placed at Brewster's angle attached to the instrument. The laser and the ion beam are made co-linear in the overlap region. The laser is then directed onto a fast Si photodetector, generating a signal for

further processing. The ion beam, meanwhile, is turned another 90° by a second deflector into a beam modulated time-of-flight (TOF) mass spectrometer. The mass spectrometer is useful for identifying all species by mass in the ion beam and as a monitor for maximizing the ion of interest.

This past year, the ion beam instrument was integrated with the same NICE-OHVMS setup described in the previous section, with the positive column discharge source now being replaced with the ion beam. Velocity modulation of the ion beam was attained by voltage-modulating a cylindrical metal drift tube which the laser and ion beams traverse. As with the positive column, NICE-OHVMS spectroscopy on the ion beam instrument was first attempted by studying the 1–0 Meinel band of N_2^+. The first signals from the instrument were obtained earlier this year, representing the first direct absorption/dispersion signal of an electronic transition in a fast ion beam. The method was improved by adjusting the velocity modulation frequency ν_{vm}, lock-in amplifier settings, ion beam energy, and other parameters to produce the optimal signal.

A typical signal is shown in Fig. 4. Since the ions are moving at 160 km/s, the transition signals are Doppler-shifted from the rest frequencies. In addition, because an optical cavity is used for signal enhancement, two laser beams are propagating through the ion beam in opposite directions. Thus, each transition is both red-shifted and blue-shifted. The NICE-OHVMS signals were fit to an equation combining NICE-OHMS with velocity modulation to determine the line centers. As with the positive column spectroscopy, very accurate line centers could be determined by fitting the equations to spectra calibrated with an optical frequency comb. Compared with the positive column line centers, the line centers determined with comb-calibrated ion spectra differed by only ∼8 MHz.

Currently, the ion beam experiment is being reconfigured to perform mid-infrared spectroscopy. A difference frequency generation (DFG) laser system has been built, producing mid-IR light at the difference frequency between the tunable Ti:sapph laser and a Nd:YAG laser. The first spectroscopic target is HN_2^+, which has been studied previously in the first generation ion beam instrument [3]. Both H_3^+ and HN_2^+ have been produced in the cold cathode source as verified by mass spectra.

Future Work

Indirect Rotational Spectroscopy

In the current setup, we intend to obtain spectra of a few molecular species in the mid-infrared with a hot ion beam. By just changing the laser from the near-infrared to the mid-infrared, we can use the same source to produce HN_2^+ as described in the previous section. Our goal is to obtain rotationally resolved lines from the ν_1 band at high accuracy using the optical frequency comb for at least the first several J states. Rotational transition frequencies will then be determined by taking combination differences of the observed transitions. Because the HN_2^+ rotational energy levels have already been determined to high accuracy [14–16], high precision indirect THz spectroscopy on HN_2^+ will be a good benchmark and test of the accuracy of the ion beam system to perform this type of spectroscopy. If the accuracy obtained from our experimental differences matches well with the transitions between levels determined previously, we can use the current setup confidently in obtaining indirect rotational data of other molecular ions of astrochemical interest (CH^+, HOC^+, HCO^+, etc.). Simple polyatomic ions such as these should be relatively easy to synthesize and detect in a hot ion beam.

Supersonic Expansion Source

As the molecular ions of interest become larger and more complex, obtaining useful spectra when these ions are at high rotational temperatures becomes difficult. As the rotational partition function increases with temperature, many rotational states become populated, and the population in any one rotational state decreases, causing the signal to become weaker. For larger molecules, this quantum dilution can be so large that spectroscopic signals drop below the sensitivity of the instrument. To lower the rotational temperature of the ion beam, we propose creating these ions in a supersonic expansion source. In such a source, precursor gas to the ion of interest is seeded in a high pressure of inert carrier gas and forced through a small hole into vacuum. The gas adiabatically expands and cools. A discharge is struck across the hole's channel length to ionize the gas. While this type

of system has been used in a pulsed regime, the aims of the project require a continuous source.

A robust continuous supersonic expansion discharge source has been built and tested previously in our lab [17] with hydrogenic discharges. For supersonically cooled ions in the ion beam, we plan to replace the current cold cathode source with this continuous supersonic source. Because we will be running the source continuously, we have a large Roots blower system with a pumping speed of 3200 L/s at 20 mTorr to evacuate the source chamber. A molecular beam skimmer will be used to extract the ion beam. To this end, we propose to have the SCS machine shop make the skimmer out of graphite, similar to a procedure found in Ref [18]. According to this article, a refractory graphite skimmer can perform in a way comparable to a commercial Ni skimmer. If these skimmers fail to extract a sufficient ion beam, we will use a commercial skimmer from Beam Dynamics [19].

To test the effectiveness of rotational cooling and skimmer extraction, spectroscopy of one of the simpler molecular ions such as HN_2^+ will be repeated. In addition, some elements of the ion beam setup will need to be rearranged, such as positions of ion optics, and a new 90° beam deflector will have to be inserted. The ion beam trajectory in several layouts of the ion optics can be modeled in SIMION [20], aiding in optimizing the supersonic source integration. Once the rotationally cooled ion beam is optimized for a familiar ion and SCRIBES is complete, we can move on to study larger, more complicated ions of more astronomical or fundamental chemical interest.

Spectroscopy of Formaldehyde Radical Cation

One molecular species of interest I propose exploring is formaldehyde radical cation, H_2CO^+. H_2CO is prevalent in the ISM, and was one of the first molecules detected in the ISM many decades ago [21]. Despite H_2CO and its protonated cation, H_2COH^+, being detected in the ISM, H_2CO^+ has not [22]. However, despite the absence of detection, the radical cation is hypothesized to play an important role in interstellar gas phase reactions.

Dalgarno and Black [23] reported the potential formation pathways as:

$$CH_3^+ + O \rightarrow H_2CO^+ + H \quad (1)$$

$$H_2CO + h\nu \rightarrow H_2CO^+ + e^- \quad (2)$$

$$H_2CO + C^+ \rightarrow H_2CO^+ + C \quad (3)$$

Destruction then occurs by the charge transfer $H_2CO^+ + M \rightarrow H_2CO + M^+$, where M is a neutral molecule of lower ionization potential. Klemperer [24] posits a main formation pathway of $H + HCO^+ \rightarrow H_2CO^+ + h\nu$, and the main destruction reaction is the aforementioned charge transfer. The charge transfer reaction, he suggests, may be the terminal reaction in a mechanism explaining formaldehyde formation in the gas phase, bringing new information to the debate on the mechanism of how organic molecules form in the ISM, i.e. on dust grains or in the gas phase [24]. Furthermore, interest has been expressed in the reaction of interstellar H_2CO with its radical cation to form more complicated, prebiotic molecules such as methyl formate, acetic acid, and glycoaldehyde [24].

Surprisingly, H_2CO^+ is not very reactive with H_2 at low temperatures. Liu et al. [25] conducted experimental and computatational studies into the $H_2CO^+ + H_2/D_2$ reaction and concluded that while the reaction pathway to H_2COH^+ and H is exothermic, the activation energy is relatively high (0.4 eV). Therefore, one may reasonably expect a significant abundance of H_2CO^+ in parts of the ISM where H_2CO and H_2COH^+ is prevalent. To look at this, I performed a calculation using the gas phase chemical model NAHOON [26] on the OSU 2005 gas phase modeling database [27] with input parameters of temperature and H atom density similar to what is observed in places where H_2COH^+ has been detected. As shown in Fig. 5, peak abundance of H_2CO^+ relative to total H reaches 5.2×10^{-8}, which is only a third less than the calculated abundance of H_2COH^+ with the same input parameters. Because H_2COH^+ is observed, and the calculated H_2CO^+ abundance is only about a third less abundant, one can reasonably conclude that there should be a high enough abundance of H_2CO^+ to detect.

Large uncertainty in the rotational energy levels of H_2CO^+ is a problem in the ability to detect this ion in the ISM. The cation has been somewhat studied computationally and by

photoelectron experiments, but, to the best of my knowledge, no high resolution rotational or rovibrational absorption spectrum has been obtained that could aid in interstellar detection. Bruna et al. [28] performed ab initio calculations of the equilibrium geometry, IR spectrum, and other properties. Further computational studies have calculated structure, harmonic frequencies, and rotational constants for the cation [29–31]. Experimentally, rotationally resolved photoelectron spectra have been obtained for H_2CO^+ [32–34], but the most accurate rotational energy levels have only been determined to within an absolute accuracy of $\sim$1.5 cm^{-1} [34]. This level of accuracy is not sufficient for effective astronomical searches.

Therefore, to aid in interstellar detection and more accurate spectroscopic knowledge of H_2CO^+, I propose that the ion beam instrument be used to obtain a highly accurate, low temperature rovibrational spectrum of H_2CO^+. Using the frequency comb as a frequency reference, we will be able to determine the rovibrational transition line centers to better than 1 MHz. With the current mid-infrared DFG laser source, we will be able to probe the ν_1 vibrational band at $\sim$2580 cm^{-1}. A simulated spectrum of this band is shown in Fig. 6, as calculated from the program Pgopher [35], using the rotational constants reported from Ref. [34]. In the previous photoelectron experiments [32–34], rotationally cooled H_2CO was produced by heating paraformaldehyde to 350–400 K, entraining the vapor in an inert gas at high pressure, supersonically expanding into a vacuum chamber, and skimming into a molecular beam [34]. We can do the same thing with the supersonic expansion discharge source, ionizing the H_2CO in the source. Roughly estimating that the ion current of H_2CO^+ will be 2/3 that of the highest N_2^+ current observed (based on integrating the supersonic expansion source and the fact that H_2CO^+ will make up a finite percentage of the total ion current), the ion density will be high enough to get a signal-to-noise ratio of $\sim$140 on just the strongest lines with no ensemble averaging, assuming a rotational temperature of 20 K. With this setup, we can obtain a high resolution rovibrational spectrum of H_2CO^+ to high accuracy, fit the spectrum, and obtain highly accurate rotational energy levels. With these accurate energy levels, the search for interstellar H_2CO^+ will be made tenable.

Conclusions

I have been a major contributor to a couple of related projects to further our group's goal of obtaining high resolution absorption spectra of astronomically and fundamentally interesting molecular ions. One project constituted the development of noise immune cavity enhanced optical heterodyne velocity modulation spectroscopy (NICE-OHVMS), a highly sensitive technique that opens a new level of detection for molecular ions. When calibrated with an optical frequency comb, NICE-OHVMS has been implemented for high precision spectroscopy of an N_2^+ plasma in a positive column discharge cell. A continuation of this project was the integration of NICE-OHVMS with an ion beam spectrometer, resulting in the first spectroscopic signal from the ion beam. Not only is this the first electronic transition of a species observed in an ion beam, but this work is a major step toward the use of the ion beam for vibrational spectroscopy of astronomically relevant molecular ions. The next steps on this project will include the benchmarking of indirect THz spectroscopy in the mid-infrared with HN_2^+, the accurate indirect THz spectroscopy of hot but simple molecular ions, and then the integration of the supersonic expansion discharge source. This integration will require the procurement, mounting, and alignment of a beam skimmer in the ion beam chamber. Once the expansion source is integrated, I propose the study of formaldehyde radical cation, H_2CO^+. Unobserved as of yet in the ISM, it is hypothesized to be involved in important interstellar chemical reactions. More accurate rotational constants and energy levels are needed for its definitive detection, and the ion beam instrument is uniquely designed for this challenge.

References

[1] C. S. Gudeman and R. J. Saykally, "Velocity modulation infrared laser spectroscopy of molecular ions," *Ann. Rev. Phys. Chem.*, vol. 35, pp. 387–418, 1984.

[2] J. V. Coe, J. C. Owrutsky, E. R. Keim, N. V. Agman, D. C. Hovde, and R. J. Saykally, "Sub-doppler direct infrared laser absorption spectroscopy in fast ion beams: The fluorine hyperfine structure of HF^+,"

[3] J. C. Owrutsky, E. R. Keim, J. V. Coe, and R. J. Saykally, "Absolute ir intensities of the ν_1 bands of HN_2^+ and HCO^+ determined by direct laser absorption spectroscopy in fast ion beams," 1989.

[4] E. R. Keim, M. L. Polak, J. C. Owrutsky, J. V. Coe, and R. J. Saykally, "Absolute infrared vibrational band intensities of molecular ions determined by direct laser absorption spectroscopy in fast ion beams," *J. Chem. Phys.*, vol. 93, pp. 3111–3119, 1990.

[5] A. A. Mills, B. M. Siller, and B. J. McCall, "Precision cavity enhanced velocity modulation spectroscopy," *Chem. Phys. Lett.*, vol. 501, pp. 1–5, 2010.

[6] B. M. Siller, A. A. Mills, and B. J. McCall, "Cavity enhanced velocity modulation spectroscopy," *Opt. Lett.*, vol. 35, pp. 1266–1268, 2010.

[7] J. Ye, *Ultrasensitive High Resolution Laser Spectroscopy and its Application to Optical Frequency Standards.* PhD thesis, University of Colorado at Boulder, 1997.

[8] J. Ye, L. Ma, and J. Hall, "Ultrasensitive detections in atomic and molecular physics: Demonstration in molecular overtone spectroscopy," *J. Opt. Soc. Am. B*, vol. 15, pp. 6–15, 1998.

[9] B. M. Siller, M. W. Porambo, A. A. Mills, and B. J. McCall, "Noise immune cavity enhanced optical heterodyne velocity modulation spectroscopy," *Opt. Ex.*, vol. 19, pp. 24822–24827, 2011.

[10] A. Foltynowicz, F. M. Schmidt, W. Ma, and O. Axner, "Noise-immune cavity-enhanced optical heterodyne molecular spectroscopy: Current status and future potential," *Appl. Phys. B*, vol. 92, pp. 313–326, 2008.

[11] W. Ma, A. Foltynowicz, and O. Axner, "Theoretical description of doppler-broadened noise-immune cavity-enhanced optical heterodyne molecular spectroscopy under optically saturated conditions," *J. Opt. Soc. Am. B*, vol. 25, pp. 1144–1155, 2008.

[12] R. W. P. Drever, J. L. Hall, F. V. Kowalski, J. Hough, G. M. Ford, A. J. Munley, and H. Ward, "Laser phase and frequency stabilization using an optical resonator," *Appl. Phys. B*, vol. 31, pp. 97–105, 1983.

[13] E. D. Black, "An introduction to pound-drever-hall laser frequency stabilization," *Am. J. Phys.*, vol. 69, pp. 79–87, 2001.

[14] R. J. Saykally, T. A. Dixon, T. G. Anderson, P. G. Szanto, and R. C. Woods, "Laboratory microwave spectrum and rest frequencies of the N_2H^+ ion," *The Astrophysical Journal*, vol. 205, pp. L101–L103, 1976.

[15] K. Sastry, P. Helminger, E. Herbst, and F. C. D. Lucia, "Millimeter and submillimeter spectra of $HN_2^+$and DN_2^+," *Chem. Phys. Lett.*, vol. 84, no. 2, pp. 286 – 287, 1981.

[16] P. Verhoeve, E. Zwart, M. Versluis, M. Drabbels, J. J. ter Meulen, W. L. Meerts, A. Dymanus, and D. B. McLay, "A far infrared laser sideband spectrometer in the frequency region 550–2700 Ghz," *Rev. Sci. Instrum.*, vol. 61, no. 6, pp. 1612–1625, 1990.

[17] K. N. Crabtree, C. A. Kauffman, and B. J. McCall, "A modular and robust continuous supersonic expansion discharge source," *Rev. Sci. Instrum.*, vol. 81, p. 086103, 2010.

[18] D. C. Jordan, R. Barling, and R. B. Doak, "Refractory graphite skimmers for supersonic free-jet, supersonic arc-jet, and plasma discharge applications," *Rev. Sci. Instrum.*, vol. 70, pp. 1640–1648, 1999.

[19] Beam Dynamics, Inc., 13749 Shelter Cove Drive, Jacksonville, FL 32225 USA, www.beamdynamicsinc.com.

[20] SIMION 3D 8.0, http://www.simion.com (2008).

[21] L. E. Snyder, D. Buhl, B. Zuckerman, and P. Palmer, "Microwave detection of interstellar formaldehyde," *Phys. Rev. Lett.*, vol. 22, pp. 679–681, Mar 1969.

[22] "Molecules in Space." I. Physikalisches Institut, Universität zu Köln, http://www.astro.uni-koeln.de/cdms/molecules.

[23] A. Dalgarno and J. H. Black, "Molecule formation in the interstellar gas," *Rep. Prog. Phys.*, vol. 39, pp. 573–612, 1976.

[24] W. Klemperer, "Astronomical chemistry," *Annu. Rev. Phys. Chem.*, vol. 62, pp. 173–184, 2011.

[25] J. Liu and S. L. Anderson, "Reaction of formaldehyde cation with molecular hydrogen: Effects of collision energy and H_2CO^+ vibrations," *J. Chem. Phys.*, vol. 120, pp. 8528–8536, 2004.

[26] V. Wakelam. NAHOON, http://www.obs.u-bordeaux1.fr/amor/VWakelam/Valentine Wakelam/Downloads.html.

[27] osu.2005, The Ohio State University Astrophysical Chemistry Group, https://www.physics.ohio-state.edu/ eric/research.html.

[28] P. J. Bruna, R. J. Hachey, and F. Grein, "The electronic structure of the H_2CO^+ radical and higher Rydberg states of H_2CO," *Mol Phys.*, vol. 94, pp. 917–928, 1998.

[29] K. C. Sears, J. W. Ferguson, T. J. Dudley, R. S. Houk, and M. S. Gordon, "Theoretical investigation of small polyatomic ions observed in inductively coupled plasma mass spectrometry: H_xCO^+ and $H_xN_2^+$ (x = 1,2,3)," *J. Phys. Chem. A*, vol. 112, pp. 2610–2617, 2008.

[30] J. W. Ferguson, T. J. Dudley, K. C. Sears, S. M. McIntyre, M. S. Gordon, and R. S. Houk, "Polyatomic ion in inductively coupled plasma-mass spectrometry part ii: Origins of N_2H^+ and H_xCO^+ ions using experimental measurements combined with calculated energies and structures," *Spectrochimica Acta Part B*, vol. 64, pp. 690–696, 2009.

[31] P. Blowers and R. I. Masel, "Calculated vibrational spectra for CH_nOH_m species," *J. Phys. Chem. A*, vol. 104, pp. 34–44, 2000.

[32] B. Niu, D. A. Shirley, and Y. Bai, "High resolution photoelectron spectroscopy and femtosecond intramolecular dynamics of H_2CO^+ and D_2CO^+," *J. Chem. Phys.*, vol. 98, pp. 4377–4390, 1993.

[33] R. T. Wiedmann, M. G. White, K. Wang, and V. McKoy, "Rotationally resolved photoionization of polyatomic hydrides: CH_3, H_2O, H_2S, H_2CO," *J. Chem. Phys.*, vol. 100, pp. 4738–4746, 1994.

[34] A. M. Schulenburg, M. Meisinger, P. P. Radi, and F. Merkt, "The formaldehyde cation: Rovibrational energy level structure and Coriolis interaction near the adiabatic ionization threshold," *J. Mol. Spectrosc.*, vol. 250, pp. 44–50, 2008.

[35] C. Western. University of Bristol. PGOPHER, a program for simulating rotational structure, http://pgopher.chm.bris.ac.uk/index.html (2009.

[36] A. A. Mills, B. M. Siller, M. W. Porambo, M. Perera, H. Kreckel, and B. J. McCall, "Ultra-sensitive high-precision spectroscopy of a fast molecular ion beam," *J. Chem. Phys.*, vol. In Press, 2011.

[37] R. Perez, J. B. Brown, Y. Utkin, J. Han, and R. F. Curl, "Observation of hot bands in the infrared spectrum of H_2CO," *J. Mol. Spectrosc.*, vol. 236, pp. 151–157, 2006.

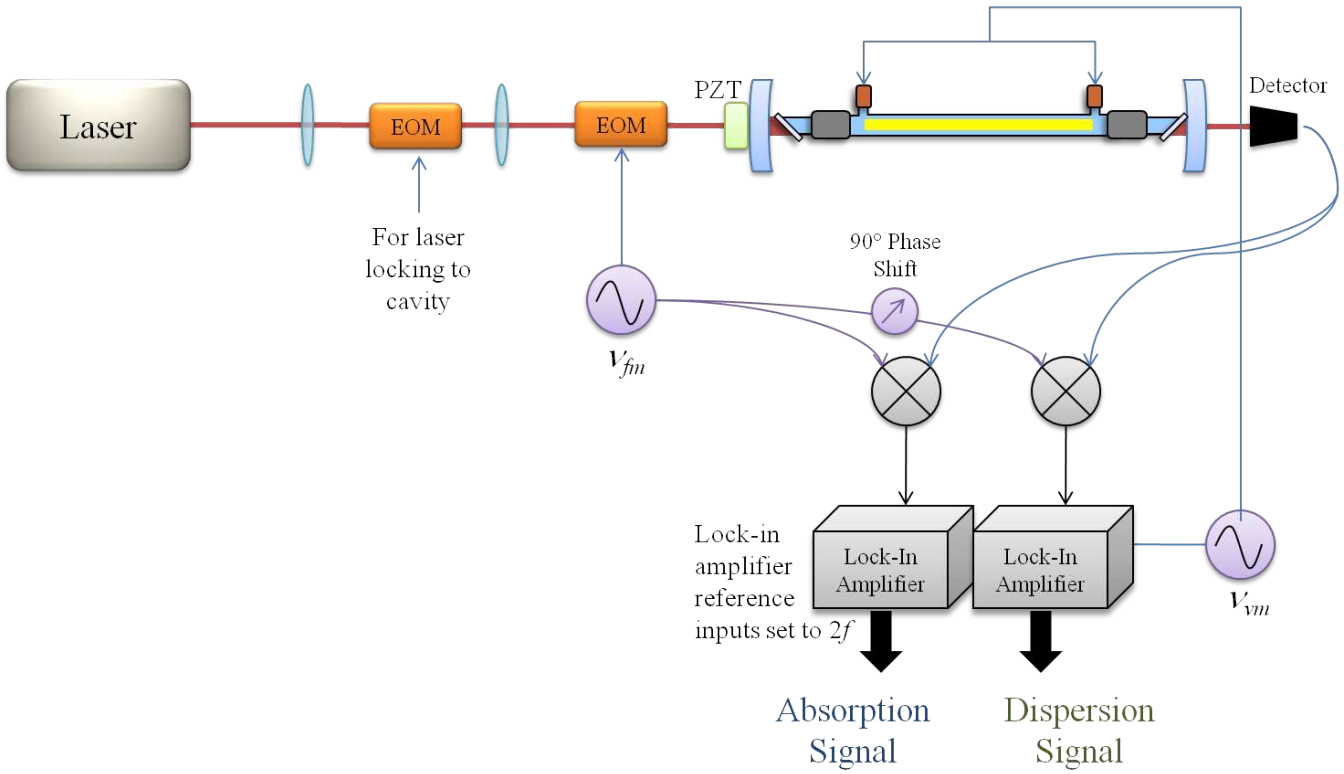

Figure 1: Diagram of NICE-OHVMS setup. PZT = piezoelectric transducer.

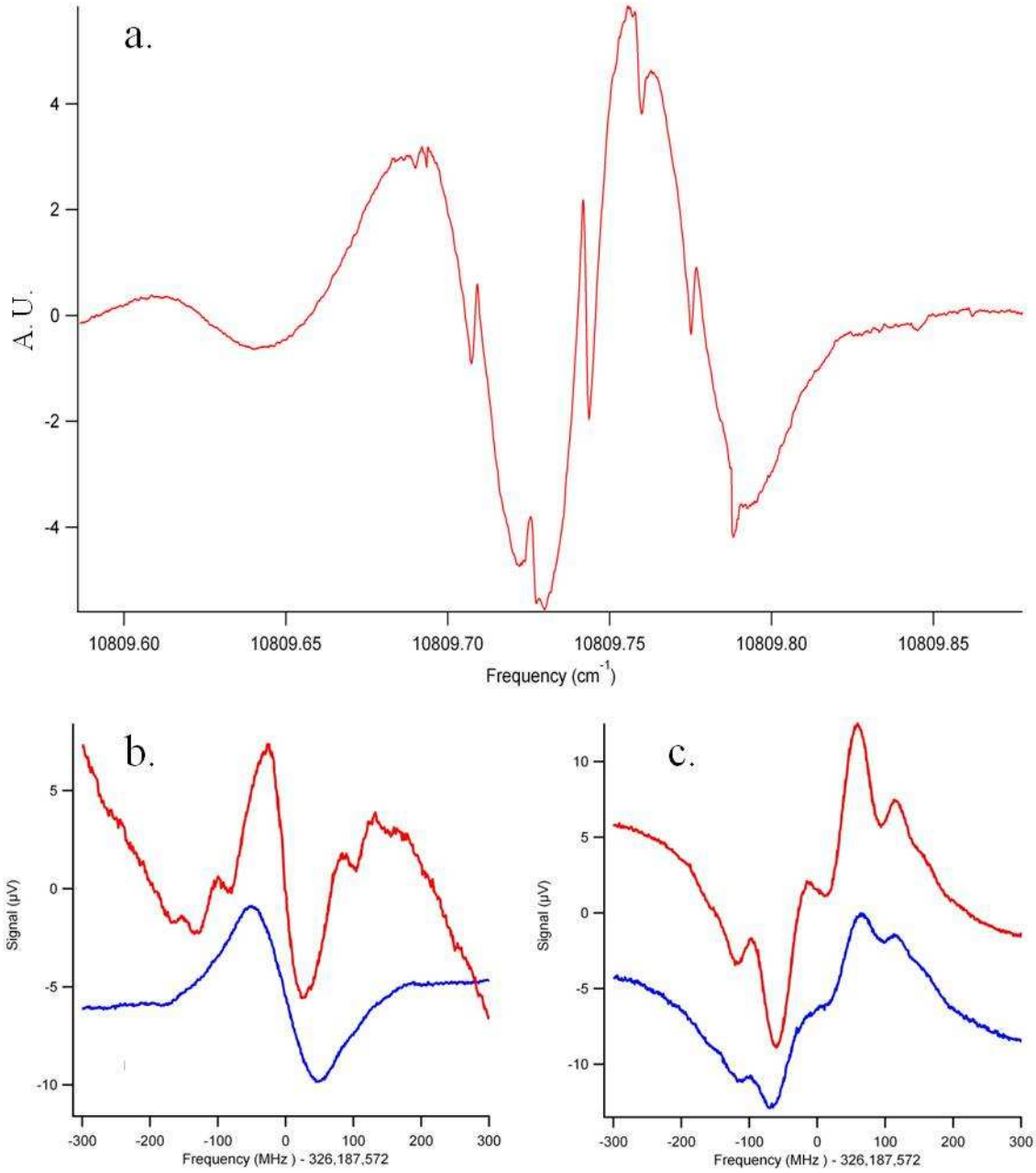

Figure 2: NICE-OHVMS spectra obtained from the 1–0 Meinel band of N_2^+ in a positive column discharge cell. a.) Doppler-broadened dispersion spectrum of the $Q_{11}(14)$ line, $\nu_{fm} = 1$ GHz. b.) Sub-Doppler dispersion spectrum of the $Q_{22}(13)$ line, $\nu_{fm} = 113$ MHz. c.) Sub-Doppler absorption spectrum of the same line with the same ν_{fm}.

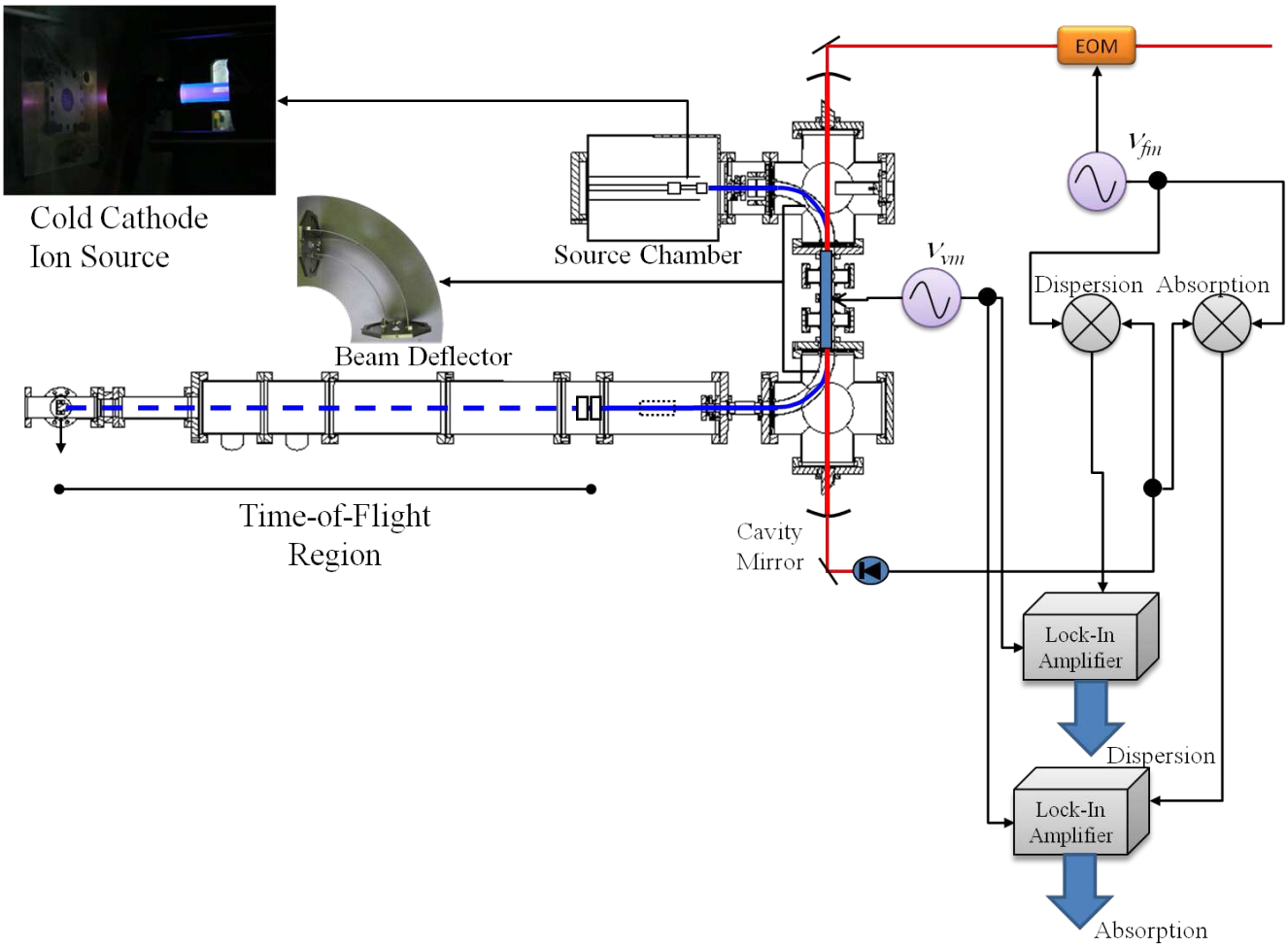

Figure 3: Basic diagram of the ion beam instrument integrated with the NICE-OHVMS technique. For a more detailed diagram, see Fig. 1 of Ref. [36].

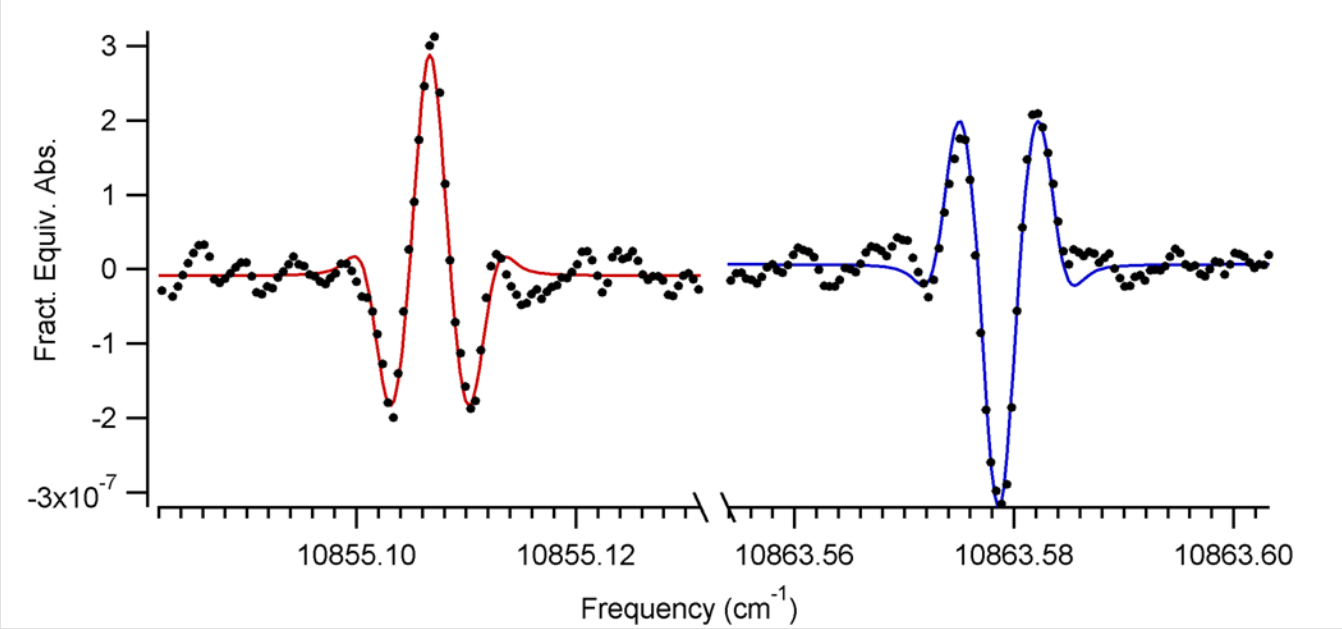

Figure 4: NICE-OHVMS dispersion signals showing the $Q_{22}(14.5)$ line of the 1–0 Meinel band of N_2^+ in the ion beam, both red- and blue-shifted. Black dots show experimental data (every 15^{th} point); colored lines show the fit to the data. Note the 180° phase difference in the signals. From Ref. [36].

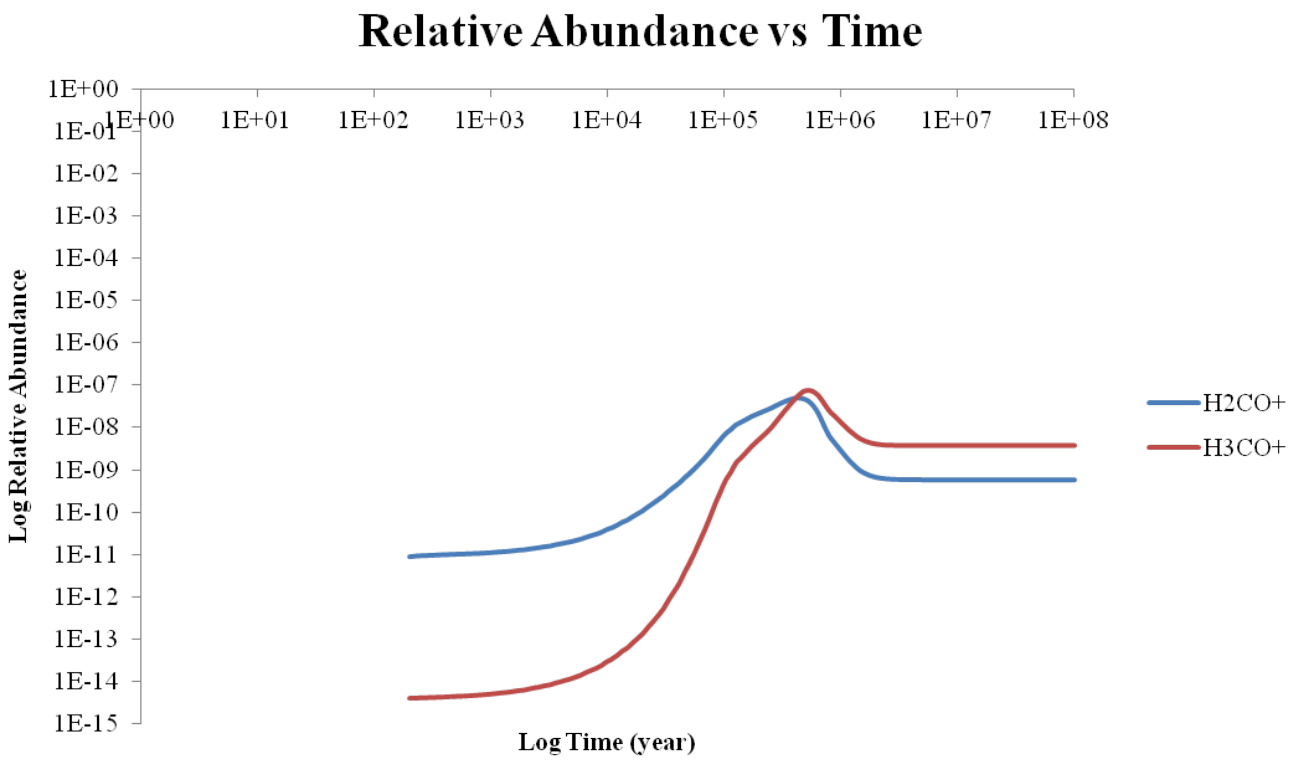

Figure 5: Relative abundances of H_2CO^+ and H_3CO^+ as a function of time as calculated from the NAHOON chemical modeling [26] program and the osu.2005 database [27]. Temperature is set to 100 K, and H density is set to 3000 cm^{-3}.

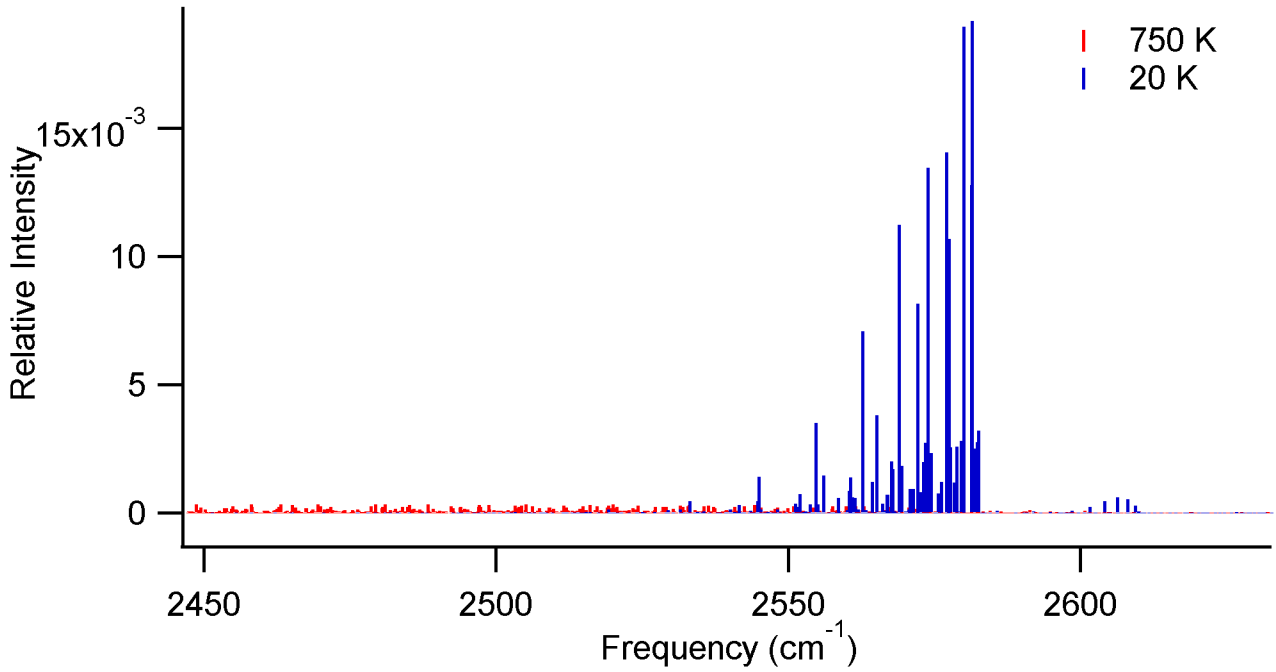

Figure 6: Simulated spectrum of the ν_1 band of H_2CO^+ at temperatures of 750 and 20 K. Band origin = 2580 cm^{-1} [32], A = 8.874 cm^{-1}, B = 1.342 cm^{-1}, C = 1.148 cm^{-1} [34]. Estimates of centrifugal distortion constants obtained from Ref. [37] and references therein.

Appendix: Paper Reprints and Preprints

1. M. Perera, B. A. Tom, Y. Miyamoto, M. W. Porambo, L. E. Moore, W. R. Evans, T. Momose, and B. J. McCall, "Refractive index measurements of solid parahydrogen," *Opt. Lett.*, vol. 36, pp. 840–842, 2011.

2. B. M. Siller, M. W. Porambo, A. A. Mills, and B. J. McCall, "Noise immune cavity enhanced optical heterodyne velocity modulation spectroscopy," *Opt. Exp.*, vol. 19, pp. 24822–24827, 2011.

3. A. A. Mills, B. M. Siller, M. W. Porambo, M. Perera, H. Kreckel, and B. J. McCall, "Ultrasensitive high-precision spectroscopy of a fast molecular ion beam," *J. Chem. Phys.*, In Press, 2011.

Refractive index measurements of solid parahydrogen

Manori Perera,[1,9] Brian A. Tom,[1,2] Yuki Miyamoto,[3,4] Michael W. Porambo,[1] Lauren E. Moore,[1,5] William R. Evans,[6] Takamasa Momose,[3,7] and Benjamin J. McCall[1,6,8,10]

[1]*Department of Chemistry, University of Illinois at Urbana–Champaign, 600 South Mathews Avenue, Urbana, Illinois 61801, USA*

[2]*Currently with the Department of Chemistry, United States Air Force Academy, Colorado 80840, USA*

[3]*Department of Chemistry, Kyoto University, Kyoto 606-8502, Japan*

[4]*Currently with Graduate School of Natural Science and Technology, Okayama University, 3-1-1, Tsushima-Naka, Okayama 700-8530, Japan*

[5]*Currently with Celanese Corporation, 9502 Bayport Boulevard, Pasadena, Texas 77507, USA*

[6]*Department of Physics, University of Illinois at Urbana–Champaign, 1110 West Green Street, Urbana, Illinois 61801, USA*

[7]*Currently with Department of Chemistry, University of British Columbia, 2036 Main Mall, Vancouver, British Columbia V6T 1Z1, Canada*

[8]*Department of Astronomy, University of Illinois at Urbana-Champaign, 1002 West Green Street, Urbana, Illinois 61801, USA*

[9]*e-mail: mperera@illinois.edu*

[10]*e-mail: bjmccall@illinois.edu*

Received December 22, 2010; accepted January 31, 2011;
posted February 11, 2011 (Doc. ID 140160); published March 9, 2011

Solid para-H_2 is a promising gain medium for stimulated Raman scattering, due to its high number density and narrow Raman linewidth. In preparation for the design of a cw solid hydrogen Raman laser, we have made the first measurements, to our knowledge, of the index of refraction of a solid para-H_2 crystal, in the wavelength range of 430–1100 nm. For a crystal stabilized at 4.4 K, this refractive index is measured to be $n_{p\text{-}H_2} = 1.130 \pm 0.001$ at 514 nm. A slight, but significant, dependence on the final crystal-growth temperature is observed, with higher $n_{p\text{-}H_2}$ at higher crystal-growth temperatures. Once a crystal is grown, it can be heated up to 10 K with no change in $n_{p\text{-}H_2}$. The refractive index varies only slightly over the observed wavelength range, and no significant birefringence was observed.

OCIS codes: 290.3030, 120.4530, 260.1180, 160.4760, 290.5910.

Molecular hydrogen has long been considered a particularly useful gain medium for stimulated Raman scattering, because of its large vibrational frequency. As early as 1986, sequential Stokes conversion in a multipass cell of gaseous H_2 was used to convert a pulsed dye laser into a continuously tunable laser in the 1–12 μm region [1]. Similar setups have been used successfully by many groups, but they depend on multipass mirrors with both high damage thresholds and high reflectivity over a wide wavelength range, which are difficult to obtain.

Solid para-H_2 has recently been demonstrated to be a suitable medium for Raman shifting pulsed lasers, without the need for specialized optics. Because of its higher density ($n \sim 2.6 \times 10^{22}$ cm^{-3}) and smaller Raman linewidth ($\Gamma \sim 7$ MHz [2]), solid H_2 would be expected to have a much higher Raman gain than gaseous H_2. Indeed, measurements by Katsuragawa and Hakuta [3] have shown that the solid's Raman gain coefficient is 7000 times higher than that of the gas. In the last decade, solid H_2 Raman pulsed lasers have been demonstrated [3–5] and are now in routine use in spectroscopic applications [6,7].

However, the high resolution spectroscopic study of molecular vibrations requires cw lasers with narrower bandwidth than can be obtained by transform-limited pulsed lasers. Carlsten *et al.* [8] have demonstrated a cw Raman laser in gaseous H_2, using a high-finesse cavity to produce sufficient intracavity power to drive the stimulated Raman scattering. Their lasers have achieved wide tunability [9] and high conversion efficiency [10], but are technically complicated due to the need for a high-finesse cavity. To our knowledge, these lasers have not been used by other groups.

Our long-term goal is to develop a cw Raman laser based on solid para-H_2. The high Raman gain of the solid should permit such a laser to have a considerably lower finesse cavity than the gaseous H_2 lasers, thereby making them easier to align and maintain. The high gain of the solid may also facilitate the extension of the cw Raman H_2 laser to longer wavelengths, where the stimulated Raman scattering process is less efficient.

To design such a laser, it is essential to minimize Fresnel losses at interfaces inside the laser cavity, in particular between the solid H_2 gain medium and the cell windows (typically sapphire) that contain the H_2 crystal. The angles of these interfaces can be chosen to be at or near Brewster's angle for minimal reflective losses, but this requires knowledge of the refractive index of solid para-H_2; to our knowledge, this quantity (which we refer to as $n_{p\text{-}H_2}$) has not been previously measured. In this Letter, we describe the procedure used independently in our labs in Illinois and Kyoto to generate a uniform para-H_2 crystal and to measure $n_{p\text{-}H_2}$. The dependence of $n_{p\text{-}H_2}$ on wavelength and the polarization angle of light, as well as the temperature of the crystal, is also discussed.

Solid para-H_2 crystals were grown in a cell (illustrated in Fig. 1) consisting of a 1.27 cm hole bored in a 5.1 cm stainless steel body. One end of the cell was machined at an angle ($\phi = 10.0°$ in Illinois; $\phi = 20.2°$ in Kyoto) to induce a deflection in a laser beam propagating through the crystal; the measurement of this deflection enabled the measurement of $n_{p\text{-}H_2}$. The ends of the cell were sealed with sapphire windows using indium gaskets. The cell was mounted to an oxygen-free high-conductivity (OFHC) copper plate machined with a small pin that

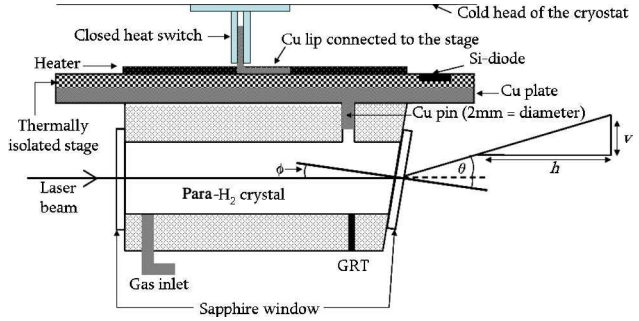

Fig. 1. (Color online) Schematic of the cell and the laser path in the presence of the para-H_2 crystal.

protrudes into the cell body (sealed with an indium gasket), to serve as a nucleation point for crystal growth. The OFHC plate in turn was mounted to the thermally isolated stage of a liquid-helium-cooled cryostat.

The temperature of the cell was controlled by adjusting the thermal contact with the cold head by opening a heat switch, and/or by using a resistive heater on the cell. The temperature gradient within the cell was monitored using a germanium resistance thermometer (GRT) mounted on the bottom of the cell and a silicon diode mounted on the thermally isolated stage where the cell rests. The temperature difference between the two sensors was typically less than 1 K, and because the thermal conductivity of solid para-H_2 (1.5 W cm^{-1} K^{-1} at 4 K [11]) is so much higher than that of stainless steel (0.003 W cm^{-1} K^{-1} [12]), the H_2 crystal would be expected to be at a temperature very close to that of the silicon diode. The cell was filled through narrow stainless steel tubing, which passed along the radiation shield of the cryostat before connecting to the cell body.

The crystal was grown with 99.98% pure para-H_2 [13] following the pressurized crystal-growth method [14], which is known to yield a transparent single crystal. Para-H_2 gas was condensed into the cell at 15–20 K, while the liquid level was watched. Once the cell was filled, the cryostat's gas line was connected to a small (150 mL) tank and the cell was heated to 30–45 K to boil off the liquid and pressurize the tank. Fresh para-H_2 gas was then condensed into the cell, and, finally, pressurized gas from the small tank (~200 psi in Illinois, ~290 psi in Kyoto) was applied to the condensed para-H_2 liquid. The temperature was slowly lowered to the final temperature over a 1 h period as the crystal grew. The crystallization was initiated from the coldest point (the copper pin at the top of the cell) and the crystal growth was observed as the liquid–solid boundary (crystallizing surface) slowly moved downward. The same procedure was repeated to create crystals with higher final growth temperatures, which required lower backing pressures [15].

Hydrogen's ability to yield such a large single crystal stems from the fact that solid para-H_2 is a quantum crystal, with a "self-annealing" property, similar to solid helium [16]. We observed a similar liquid–solid boundary during crystal growth as in previous studies ([14], Fig. 2), and our observation of a single crystallizing surface is strong evidence that a single crystal was in fact formed. In other trial runs (with different crystal-growth procedures, inadequate backing pressure, or impurities in the sample), a single crystallizing surface was not observed: the resulting samples were not completely transparent; laser beams sent through those samples suffered complex scattering patterns, and cracks would result as the temperature dropped, separating individual crystals. With proper care in the crystal-growth process, however, a transparent single crystal always resulted. Previous work has established that high purity para-H_2 crystallizes to form a hexagonal close-packed lattice at low temperature and high pressure [15] and that the c axis follows the largest thermal gradient [4,17]; in the present case this is the vertical axis.

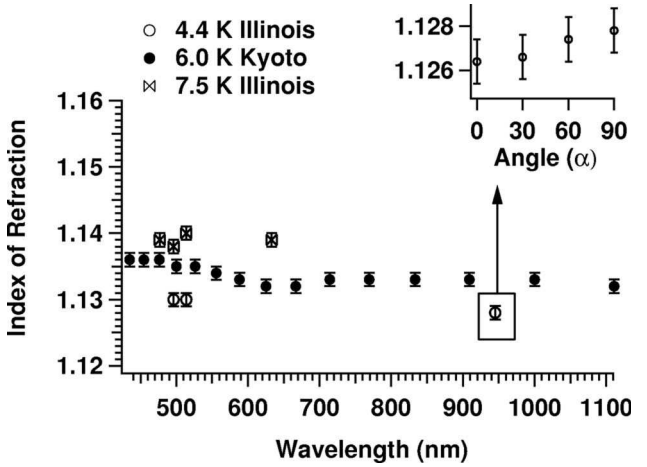

Fig. 2. Index of refraction data taken at various growth temperatures of the crystal. The inset shows the dependence on α, the angle (in degrees) between the polarization axis of the light and the c axis of the crystal.

The optical setup used for measurements of $n_{p\text{-}H_2}$ in Illinois consisted of three lasers: an argon ion laser with 476, 496, and 514 nm emission; a He–Ne laser with 632 nm emission; and a tunable diode laser at 945 nm. After the crystal was fully grown, the laser light was passed through the crystal. The angle of the deflected beam (θ) was determined by measuring its distance (labeled v) from the horizontal at two positions separated by 1.5 m (labeled h), as shown in Fig. 1. The beam position was determined by monitoring the voltage of a photodiode as it was translated vertically. The measured beam positions are accurate to within ±0.013 cm, the precision of the micrometer mount used. In Kyoto, a master oscillator power oscillator laser was used to measure $n_{p\text{-}H_2}$ at 15 different wavelengths between 430 nm and 1100 nm. In that measurement, the deflected angle (θ) was measured by locating the laser spot (visually) on a screen 6.5 m from the cryostat.

Snell's law, $n_{p\text{-}H_2}\sin(\phi) = n_{\text{vac}}\sin(\theta+\phi)$, was used to infer $n_{p\text{-}H_2}$. Here, ϕ includes both the tilt of the cryostat stage with respect to the incident laser beam as well as the angle of the intentionally tilted window. The dependence of $n_{p\text{-}H_2}$ on the polarization angle of the incident laser was measured by inserting a half-wave plate in the laser path prior to the cryostat and changing its angle in increments of 15°. The results are presented in Fig. 2.

The measurements show only a slight dependence of $n_{p\text{-}H_2}$ on wavelength. The 6.0 K data, which have the largest wavelength coverage, show that $n_{\text{p}\text{-}H_2}$ decreases slightly with increasing wavelength up to ~650 nm and then levels off, becoming consistent with a constant

value of 1.132±0.001. The 4.4 K and 7.5 K data sets are each consistent with a constant $n_{p\text{-}H_2}$, but these data have sparser wavelength coverage. The constancy of $n_{p\text{-}H_2}$ with wavelength is expected, since para-H_2 has no absorptions between the far-IR and the UV.

The inset of Fig. 2 shows how $n_{p\text{-}H_2}$ varies with the polarization angle, α, of the incoming laser beam (at 945 nm and 4.4 K). Although there is a hint of an increase of $n_{p\text{-}H_2}$ with α, the trend is not statistically significant, given our measurement uncertainties; we adopt an upper limit of 0.002 for the magnitude of birefrigence.

The data indicate that $n_{p\text{-}H_2}$ increases with the final temperature of crystal growth. This is surprising, as the density of solid para-H_2 is known [14,15] to decrease slightly with increasing temperature in this range. One might therefore anticipate that $n_{p\text{-}H_2}$ would decrease with decreasing density (as the temperature increases), but our observations show that $n_{p\text{-}H_2}$ instead increases.

To test the sensitivity of $n_{p\text{-}H_2}$ to the rate of crystal growth, we grew a crystal at a faster rate, lowering the temperature to 4.4 K in only 10 min, rather than 1 h. This crystal had a slightly higher $n_{p\text{-}H_2}$ (at 514 nm) of 1.134 ± 0.001, compared with 1.130 ± 0.001 for the slowly grown crystal. One might expect the slowly grown crystal to attain a higher density than the quickly grown crystal, as the former has more time to rearrange its lattice. These observations are consistent with the other measurements, in the sense that in both cases $n_{p\text{-}H_2}$ increases with decreasing density (due to either higher growth temperature or faster growth rate).

After crystal growth is complete, raising the temperature does not change $n_{p\text{-}H_2}$. For a crystal stabilized at a final growth temperature of 4.4 K, we gradually increased the temperature up to 10 K (in increments of ~0.5 K) and observed no change in the deflection of the laser. Once the crystal is completely grown, the lattice cannot expand because it is completely confined in the cell, and the constant density leads to a constant $n_{p\text{-}H_2}$.

The observed temperature dependence of $n_{p\text{-}H_2}$ is significantly larger than can be accounted for by the measurement uncertainties. For example, in order for the measured $n_{p\text{-}H_2}$ of the 4.4 K crystal to fall within the uncertainties of the data at 6.0 K, the measured deflection angle would have to have been mismeasured by 0.14°, which corresponds to an error in the vertical beam deflection (v) of 0.23 cm, or 18 times our precision. We therefore conclude that the surprising inverse dependence of $n_{p\text{-}H_2}$ on density is not due to systematic errors in the measurements, but we cannot offer a physical explanation of the effect at this time.

In summary, we have measured the refractive index of solid para-H_2 for the first time, to our knowledge. Measurements were performed for final crystal-growth temperatures of 4.4, 6.0, and 7.5 K, over a wavelength range of 430–1100 nm. The refractive index (at 514 nm) is $n_{p\text{-}H_2} = 1.130 \pm 0.001$ for a crystal stabilized at 4.4 K and increases to 1.140 ± 0.001 at 7.5 K. Our measurements suggest that $n_{p\text{-}H_2}$ is dependent on the density of the crystal, with higher values at lower densities. A small dependence of $n_{p\text{-}H_2}$ on wavelength was observed, but no significant dependence on polarization was seen. These measurements can be expected to facilitate the development of a cw Raman laser using solid para-H_2 as the gain medium, which may ultimately lead to a new widely tunable and narrow linewidth laser source in the mid-IR region.

The authors wish to thank Siddhartha Bhasker for his assistance with the early stages of the experimental development in Illinois. The work in Illinois has been supported by the David and Lucile Packard Foundation and by the University of Illinois.

References

1. P. Rabinowitz, B. N. Perry, and N. Levinos, IEEE J. Quantum Electron. **22**, 797 (1986).
2. T. Momose, D. P. Weliky, and T. Oka, J. Mol. Spectrosc. **153**, 760 (1992).
3. M. Katsuragawa and K. Hakuta, Opt. Lett. **25**, 177 (2000).
4. M. Fushitani, S. Kuma, Y. Miyamoto, H. Katsuki, T. Wakabayashi, T. Momose, and A. F. Vilesov, Opt. Lett. **28**, 37 (2003).
5. B. J. McCall, A. J. Huneycutt, R. J. Saykally, C. M. Lindsay, T. Oka, M. Fushitani, Y. Miyamoto, and T. Momose, Appl. Phys. Lett. **82**, 1350 (2003).
6. K. E. Kuyanov, T. Momose, and A. F. Vilesov, Appl. Opt. **43**, 6023 (2004).
7. H. Hoshina, D. Skvortsov, B. G. Sartakov, and A. F. Vilesov, J. Chem. Phys. **132**, 074302 (2010).
8. J. K. Brasseur, K. S. Repasky, and J. L. Carlsten, Opt. Lett. **23**, 367 (1998).
9. L. S. Meng, K. S. Repasky, P. A. Roos, and J. L. Carlsten, Opt. Lett. **25**, 472 (2000).
10. L. S. Meng, P. A. Roos, K. S. Repasky, and J. L. Carlsten, Opt. Lett. **26**, 426 (2001).
11. R. G. Bohn and C. F. Mate, Phys. Rev. B **2**, 2121 (1970).
12. NIST Cryogenic Technologies Group, Material Properties Compilation, available at: http://cryogenics.nist.gov.
13. B. A. Tom, S. Bhasker, Y. Miyamoto, T. Momose, and B. J. McCall, Rev. Sci. Instrum. **80**, 016108 (2009).
14. M. Suzuki, M. Katsuragawa, R. S. D. Sihombing, J. Z. Li, and K. Hakuta, J. Low Temp. Phys. **111**, 463 (1998).
15. P. C. Souers, *Hydrogen Properties for Fusion Energy* (University of California, 1986).
16. T. Momose, J. Low Temp. Phys. **111**, 469 (1998).
17. D. P. Weliky, K. E. Kerr, T. J. Byers, Y. Zhang, T. Momose, and T. Oka, J. Chem. Phys. **105**, 4461 (1996).

Noise immune cavity enhanced optical heterodyne velocity modulation spectroscopy

Brian M. Siller,[1] Michael W. Porambo,[1] Andrew A. Mills[1] and Benjamin J. McCall[1,2,*]

[1]*Department of Chemistry, University of Illinois at Urbana-Champaign, Urbana, IL, 61801*
[2]*Departments of Astronomy and Physics, University of Illinois at Urbana-Champaign, Urbana, IL, 61801*
[*]*bjmccall@illinois.edu*

http://bjm.scs.illinois.edu/

Abstract: The novel technique of cavity enhanced velocity modulation spectroscopy has recently been demonstrated as the first general absorption technique that allows for sub-Doppler spectroscopy of molecular ions while retaining ion-neutral discrimination. The previous experimental setup has been further improved with the addition of heterodyne detection in a NICE-OHMS setup. This improves the sensitivity by a factor of 50 while retaining sub-Doppler resolution and ion-neutral discrimination. Calibration was done with an optical frequency comb, and line centers for several N_2^+ lines have been determined to within an accuracy of 300 kHz.

OCIS codes: (300.1030) Absorption; (300.6320) Spectroscopy, high-resolution; (300.6460) Spectroscopy, saturation; (300.6380) Spectroscopy, modulation; (300.6390) Spectroscopy, molecular; (300.6340) Spectroscopy, infrared.

References and links

1. S. K. Stephenson and R. J. Saykally, "Velocity modulation spectroscopy of ions," Chem. Rev. **105**, 3220–3234 (2005).
2. B. M. Siller, A. A. Mills, and B. J. McCall, "Cavity-enhanced velocity modulation spectroscopy," Opt. Lett. **35**, 1266–1268 (2010).
3. A. A. Mills, B. M. Siller, and B. J. McCall, "Precision cavity enhanced velocity modulation spectroscopy," Chem. Phys. Lett. **501**, 1 – 5 (2010).
4. J. Ye, L. S. Ma, and J. L. Hall, "Ultrasensitive detections in atomic and molecular physics: demonstration in molecular overtone spectroscopy," J. Opt. Soc. Am. B **15**, 6–15 (1998).
5. A. Foltynowicz, F. M. Schmidt, W. Ma, and O. Axner, "Noise-immune cavity-enhanced optical heterodyne molecular spectroscopy: Current status and future potential," Appl. Phys. B **92**, 313–326 (2008).
6. R. D. L. Kronig, "On the theory of dispersion of x-rays," J. Opt. Soc. Am. **12**, 547–556 (1926).
7. A. Foltynowicz, W. Ma, F. M. Schmidt, and O. Axner, "Wavelength-modulated noise-immune cavity-enhanced optical heterodyne molecular spectroscopy signal line shapes in the Doppler limit," J. Opt. Soc. Am. B **26**, 1384–1394 (2009).
8. E. A. Donley, T. P. Heavner, F. Levi, M. O. Tataw, and S. R. Jefferts, "Double-pass acousto-optic modulator system," Rev. Sci. Instrum. **76**, 063112 (2005).
9. R. W. P. Drever, J. L. Hall, F. V. Kowalski, J. Hough, G. M. Ford, A. J. Munley, and H. Ward, "Laser phase and frequency stabilization using an optical-resonator," Appl. Phys. B **31**, 97–105 (1983).
10. W. Ma, A. Foltynowicz, and O. Axner, "Theoretical description of doppler-broadened noise-immune cavity-enhanced optical heterodyne molecular spectroscopy under optically saturated conditions," J. Opt. Soc. Am. B **25**, 1144–1155 (2008).

#151471 - $15.00 USD Received 28 Jul 2011; revised 10 Oct 2011; accepted 17 Oct 2011; published 18 Nov 2011

11. M. S. Child, *Molecular Collision Theory* (Academic Press Inc, 1974).
12. R. G. DeVoe and R. G. Brewer, "Laser-frequency division and stabilization," Phys. Rev. A. **30**, 2827–2829 (1984).

1. Introduction

1.1. Velocity modulation spectroscopy

Laboratory spectroscopy of molecular ions is of great interest to a variety of fields, but is typically difficult because even in laboratory plasmas designed to observe a particular ion, the ion of interest has a very low concentration, typically orders of magnitude lower than that of any ambient neutral molecules in discharge cells. Velocity Modulation Spectroscopy (VMS) in positive column discharge cells has been the most commonly used technique in this field over the past few decades because it combines the advantages of relatively high ion density and ion-neutral discrimination [1].

Recently, a new method of performing VMS has been demonstrated by placing the plasma discharge cell within an optical cavity in a technique we call Cavity Enhanced Velocity Modulation Spectroscopy (CEVMS) [2, 3]. The optical cavity provides two major advantages over traditional VMS: greatly increased path length (about an order of magnitude greater than any previous VMS experiments, even with a cavity finesse of only 300) and the ability to observe a sub-Doppler Lamb dip for each spectral line (due to the high intracavity laser power and the perfectly overlapped counterpropagating beams induced by the optical cavity).

Although CEVMS showed much promise, its sensitivity was ultimately limited by noise in the laser-cavity lock, particularly noise that was induced by the high voltage AC plasma discharge. In the current work, the sensitivity limitations of CEVMS have been greatly improved by combining the technique with Noise Immune Cavity Enhanced Optical Heterodyne Molecular Spectroscopy (NICE-OHMS).

1.2. NICE-OHMS

NICE-OHMS is a technique that was first developed in the late 1990s [4], and has since been used with great success by several groups to observe spectra of many different neutral molecules with sensitivity unprecedented by other direct absorption spectroscopic techniques [5].

The principle of NICE-OHMS is that while the laser carrier frequency is locked to an optical cavity mode, a set of FM sidebands are added to the laser, spaced at an integer multiple of the cavity free spectral range (FSR). Thus the carrier (laser center frequency) and both sidebands get coupled into, and out of, the cavity simultaneously. The transmitted beam is detected with a fast photodiode and demodulated at the heterodyne modulation frequency.

Because the two sidebands have the same intensity when no absorbers are present within the cavity and are 180° out of phase with one another, the positive and negative RF beat signals created by the sideband frequencies beating against the carrier frequency cancel each other out, causing NICE-OHMS to be a zero-background technique. When the frequency modulated laser is coupled through the optical cavity and the sideband spacing is set to be exactly equal to the cavity FSR, any noise in the laser-cavity lock is the same for the carrier and both sidebands, so the demodulated signal is unaffected. Thus, NICE-OHMS allows for the path length enhancement of an optical cavity, a factor of $(2 \cdot Finesse/\pi)$, while not introducing any additional noise in the system beyond that of ordinary single-pass heterodyne spectroscopy.

An absorption signal is observed when one of the RF sidebands is absorbed more than the other, causing an imbalance in the two heterodyne beats, so they no longer add to zero. For any absorption, there is a corresponding dispersion, related by the Kramers-Kronig relations [6]. With heterodyne detection, it is possible to observe this dispersion signal, because a phase shift

#151471 - $15.00 USD Received 28 Jul 2011; revised 10 Oct 2011; accepted 17 Oct 2011; published 18 Nov 2011

in the carrier frequency or either of the sideband frequencies also creates an imbalance in the beat signals, leading to a net signal. The net signal obtained from a phase shift of one of the laser frequencies is 90° out of phase with that obtained from absorption of one of the sidebands, so through phase-sensitive detection, it is possible to observe absorption and dispersion independently of one another.

2. Experimental

The experimental setup is shown in Fig. 1. It is similar to that previously used for cavity-enhanced velocity modulation experiments [2, 3], with the addition of a second electro optic modulator (EOM) and a high speed photodiode for heterodyne detection.

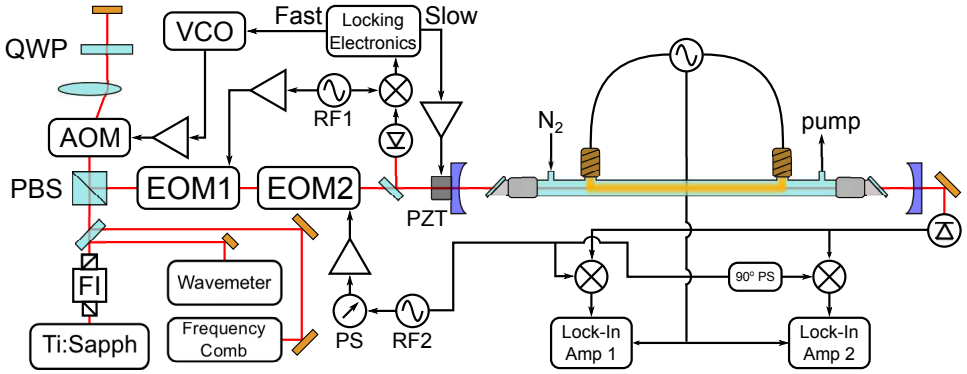

Fig. 1. Experimental Layout. FI: Faraday isolator; PBS: polarizing beamsplitter; AOM: acousto optic modulator; QWP: quarter wave plate; VCO: voltage controlled oscillator; EOM: electro optic modulator; PZT: piezo electric transducer; RF: radio frequency generator; PS: phase shifter.

The laser is double-passed through an acousto optic modulator that is resonant at 85 MHz, which red-shifts the laser frequency by 170 MHz and makes the pointing of the beam immune to changes in the acousto optic modulator (AOM) drive frequency [8].

The laser is then passed through two electro optic modulators, which add two sets of RF sidebands to the laser frequency. The first EOM, which is non-resonant, adds 30 MHz sidebands with a small modulation index ($\beta \sim 0.01$). These sidebands are detected in the back-reflected signal off of the cavity, and are demodulated with an RF mixer to generate a Pound-Drever-Hall [9] error signal. That error signal is then processed with analog electronics, and split off into two components; slow corrections (up to 100 Hz) are sent to the cavity piezo, while faster corrections (up to 60 kHz) are sent to the voltage controlled oscillator (VCO) that drives the acousto optic modulator AOM.

The second EOM, which is resonant, adds sidebands spaced at an integer multiple of the FSR of the optical cavity. The light transmitted through the cavity is detected with a fast photodiode. The AC portion of the detector signal is sent through an RF amplifier, then a power splitter that sends the signal to two mixers. The mixers are referenced to the sideband RF signal, but are set to be 90° out of phase with one another through a phase delay induced by a difference in cable lengths between the reference signal and the local oscillator (LO) input of the mixers. The overall detection phase is adjusted using an RF phase shifter in the line between the RF generator and the amplifier that drives the heterodyne EOM.

Two different experimental setups were used to observe several lines in the $v = 1 \leftarrow 0$ band of the Meinel system ($A^2\Pi_u - X^2\Sigma_g^+$) of N_2^+. One setup used a 1 GHz resonant EOM to space the

#151471 - $15.00 USD Received 28 Jul 2011; revised 10 Oct 2011; accepted 17 Oct 2011; published 18 Nov 2011

heterodyne sidebands at 9 cavity FSRs for observation of Doppler profiles and demonstration of ion-neutral discrimination. The other setup used a 113 MHz resonant EOM to space the sidebands at 1 cavity FSR for sub-Doppler studies of the observed Lamb dips.

The optical cavity used in both setups had a finesse of 300, which gave a cavity linewidth of 450 kHz. Throughout the course of a scan, the cavity length would change by 12 μm as the piezo was scanned, causing the FSR to change by approximately 1 kHz. To avoid increased noise near the end of the piezo travel, a feed-forward loop was implemented, in which the piezo voltage was scaled down, inverted, and sent to the DC FM input of the RF driver so the sideband spacing would track with the cavity FSR as the cavity length was scanned.

3. Results & discussion

3.1. Sub-Doppler lineshape analysis

Each laser frequency present in the cavity can act as a pump and/or a probe for sub-Doppler spectroscopy. For example, the carrier can act as a pump while a sideband acts as a probe, producing a Lamb dip spaced halfway between the two frequencies. Thus, Lamb dips are observed spaced at half the sideband spacing. For significant modulation depth ($\beta \sim 1$), where maximum heterodyne signal intensity is obtained, second-order sidebands also add small contributions to the outer edges of the signals. The overall sub-Doppler lineshape function is given by

$$\begin{aligned}\chi(\nu_d) = \{&A_1[\chi_a(\nu_d - \frac{\nu_{fm}}{2}) - \chi_a(\nu_d + \frac{\nu_{fm}}{2})] + A_2[\chi_a(\nu_d - \nu_{fm}) - \chi_a(\nu_d + \nu_{fm})] \\ &+ A_3[\chi_a(\nu_d - \frac{3\nu_{fm}}{2}) - \chi_a(\nu_d + \frac{3\nu_{fm}}{2})]\} \sin\theta_{fm} \\ &+ \{A_0[\chi_d(\nu_d)] + A_1[\chi_d(\nu_d - \frac{\nu_{fm}}{2}) + \chi_d(\nu_d + \frac{\nu_{fm}}{2})] \\ &+ A_2[\chi_d(\nu_d - \nu_{fm}) + \chi_d(\nu_d + \nu_{fm})]\} + A_3[\chi_d(\nu_d - \frac{3\nu_{fm}}{2}) + \chi_d(\nu_d + \frac{3\nu_{fm}}{2})]\} \cos\theta_{fm}\end{aligned} \tag{1}$$

where $\nu_d = \nu - \nu_0$ is the detuning of the laser center frequency, ν, from the transition center frequency, ν_0. ν_{fm} is the heterodyne modulation frequency and θ_{fm} is the heterodyne detection phase. $A_{0,1,2,3}$ are amplitudes related to the overall laser power and the modulation depth. In this work, these amplitudes are used as fit parameters with the constraint $A_i > A_{i+1}$.

χ_a and χ_d are general lineshape functions for absorption and dispersion profiles, respectively. In this work, the Lamb dips appear to be Gaussian, so χ_a is the general peak-normalized Gaussian lineshape, while χ_d is derived from χ_a transformed by the Kramers-Kronig relations [6]. The lineshape functions are given by [7]

$$\chi_a(\nu) = e^{-4\gamma^2} \qquad \text{and} \qquad \chi_d(\nu) = \frac{2}{\sqrt{\pi}} e^{-\gamma^2} \int_0^\gamma e^{\gamma'^2} d\gamma' \tag{2}$$

where w is the Gaussian full width at half maximum (FWHM), ν_0 is the line center, and $\gamma = 2(\ln 2)^{1/2}(\nu - \nu_0)/w$.

The combination of concentration and velocity modulation of N_2^+ causes the observed Doppler profile to be much different from those seen in other NICE-OHMS setups that observe neutral molecules. In this work, no attempt was made at fitting the overall Doppler broadened lineshapes; the Doppler broadened profile was approximated by a third order polynomial near the line center that was used as a baseline for sub-Doppler fitting.

3.2. 1 GHz sideband spacing

The 1 GHz system, with sidebands spaced at 9 FSRs, was used for Doppler-broadened scans. Figure 2 shows a typical scan with this system, collected with a 300 ms lock-in time constant,

#151471 - $15.00 USD Received 28 Jul 2011; revised 10 Oct 2011; accepted 17 Oct 2011; published 18 Nov 2011

100 ms delay between points, and approximately 10 MHz step size. With this setup, only a single mixer and lock-in amplifier were used, and the RF phase was set to be nearly pure dispersion, as evidenced by the presence of a strong central Lamb dip, which is expected to be absent from the pure absorption signal.

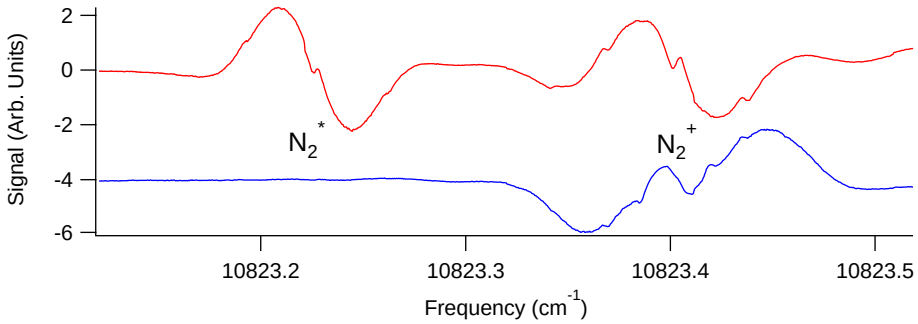

Fig. 2. A scan with 1 GHz sideband spacing, demonstrating discrimination between N_2^+ and N_2^*. At the left is an unassigned transition of electronically excited neutral N_2. At the right is an unresolved blend of two N_2^+ lines, $Q_{12}(6)$ and $Q_{11}(14)$. The top and bottom traces are the X and Y channels of the lock-in amplifier, rotated in post-processing by 64°.

During data collection, the lock-in amplifier phase was set to zero. After collection of the data, computer software was used to rotate the phase of the signal with respect to the plasma frequency in order to minimize the amount of N_2^* signal present in the Y channel. Note that just the concentration of N_2^* is modulated in the plasma, so its Doppler-broadened profile is similar to other NICE-OHMS lineshapes that are typically observed for neutral molecules [10]. With N_2^+, however, both the velocity and concentration are being modulated simultaneously, which leads to a more complex lineshape that cannot be isolated into a single phase.

3.3. 113 MHz sideband spacing

For spectroscopy with sidebands spaced at a single cavity FSR, both RF mixers were used, and the lengths of cables going to the LO inputs of the two mixers were made such that the relative phases were 90° apart. The overall phase of the system was adjusted to optimize the isolation of absorption and dispersion signals using an electronic phase shifter on the input to the amplifier that drives EOM2.

A typical scan with the 113 MHz system, calibrated with an optical frequency comb, as described in [3], is shown in Fig. 3. A single scan produces four orthogonal signals: absorption and dispersion, each with X and Y components. Absorption and dispersion signals are first separated using the 90° phase difference in the RF mixer references, then each of these is split into two components separated by 90° relative to the plasma frequency by mixers within the lock-in amplifiers. Fits were performed on the Lamb dips of the comb-calibrated scans using Eq. (1), along with a cubic sloped baseline to approximate the Doppler profile near the line center. Note that the residuals show that the actual lineshape is more complex than that given in Eq. (1) due to the combination of concentration modulation and velocity modulation occurring in the plasma. A more thorough lineshape analysis will be the subject of future studies.

Based on fits of several scans in alternating directions, calibrated with an optical frequency comb, the measured line center frequency was found to have a standard deviation of approximately 2 MHz. Because of the delayed response of the lock-in amplifiers used for demodulation, the determined line centers tend to be shifted in the direction of the scanning. By pairing

#151471 - $15.00 USD Received 28 Jul 2011; revised 10 Oct 2011; accepted 17 Oct 2011; published 18 Nov 2011

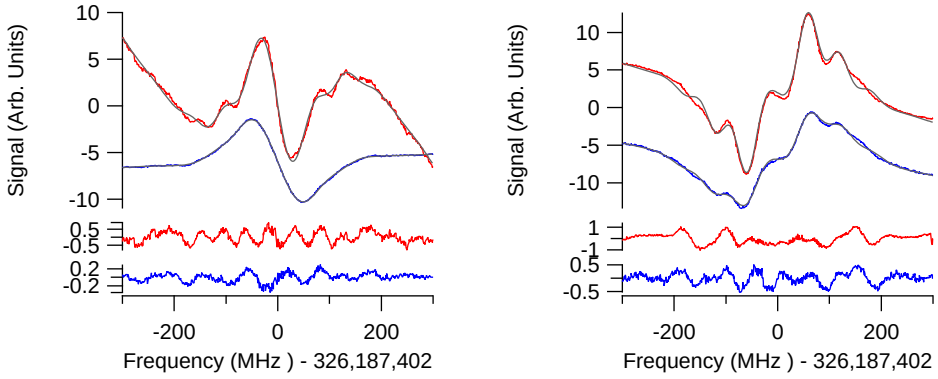

Fig. 3. Dispersion (left) and absorption (right) Lamb dips of the $Q_{22}(13)$ line of N_2^+ observed in the 113 MHz configuration, calibrated with an optical frequency comb. Top, red: Y channel outputs of lock-ins. Bottom, blue: X channel outputs of lock-ins, offset vertically for clarity. Residuals are shown at the bottom.

and averaging pairs of scans in opposite directions, the measurement standard deviation can be reduced to ∼300 kHz. It was found that the line center frequencies determined previously in Ref [3] were all too high by 20 MHz due to an ambiguity in the determination of the sign of the comb carrier-envelope offset.

The pressure broadening of ∼8 MHz/Torr of the observed Lamb dips observed in Ref [3] and in the current work is consistent with the expected broadening given by the total collision cross section given by Eq. (5.69) of Ref [11] integrated over the Maxwell-Boltzmann distribution for the estimated plasma temperature (∼600 K), but the extrapolated ∼32 MHz linewidth at zero pressure is still not fully understood.

4. Conclusions & future work

The technique of cavity enhanced velocity modulation spectroscopy has been further improved by the addition of heterodyne detection to minimize the noise induced by the laser-cavity lock. This modification has improved upon the achievable sensitivity of CEVMS by nearly two orders of magnitude while retaining ion-neutral discrimination. Combined with an optical frequency comb, line centers can be determined to within 300 kHz.

Further improvement to this technique can be realized by moving to a higher finesse cavity to increase both the effective path length and the intracavity optical power. Moving to a higher finesse cavity would cause this technique to be more sensitive to mismatches in the cavity FSR and RF sideband frequency due to the narrower cavity resonances. This effect could be compensated for by actively locking the RF sideband frequency to the cavity FSR using the DeVoe-Brewer [12] method, rather than the less precise feed-forward loop that was used in this work. This technique could also be extended to mid-infrared wavelengths by using a high power optical parametric oscillator (OPO) to observe a much greater variety of molecular ions.

Acknowledgments

This work has been supported by an NSF CAREER award (CHE 04-49592), an Air Force Young Investigator award (FA9550-07-1-0128), the NASA Laboratory Astrophysics program (NNX08AN82G), a David and Lucile Packard Fellowship, and the University of Illinois. Michael Porambo has been supported by a Robert C. and Carolyn J. Springborn Fellowship.

#151471 - $15.00 USD Received 28 Jul 2011; revised 10 Oct 2011; accepted 17 Oct 2011; published 18 Nov 2011

Ultra-sensitive high-precision spectroscopy of a fast molecular ion beam

Andrew A. Mills,[1] Brian M. Siller,[1] Michael W. Porambo,[1] Manori Perera,[1, a)] Holger Kreckel,[1] and Benjamin J. McCall[1, 2, b)]

[1)] *Department of Chemistry, University of Illinois, Urbana, Illinois 61801, USA*

[2)] *Departments of Physics and Astronomy, University of Illinois, Urbana, Illinois 61801, USA*

(Dated: 9 October 2011)

Direct spectroscopy of a fast molecular ion beam offers many advantages over competing techniques, including the generality of the approach to any molecular ion, the complete elimination of spectral confusion due to neutral molecules, and the mass-identification of individual spectral lines. The major challenge is the intrinsic weakness of absorption or dispersion signals resulting from the relatively low number density of ions in the beam. Direct spectroscopy of an ion beam was pioneered by the Saykally group in the late 1980s, but has not been attempted since that time. Here, we present the design and construction of an ion beam spectrometer with several improvements over the Saykally design. The ion beam and its characterization have been improved by adopting recent advances in electrostatic optics, along with a time-of-flight mass spectrometer that can be used simultaneously with optical spectroscopy. As a proof of concept, a noise-immune cavity-enhanced optical heterodyne molecular spectroscopy (NICE-OHMS) setup with a noise equivalent absorption of $\sim 2 \times 10^{-11}\,\mathrm{cm^{-1}\,Hz^{-1/2}}$ has been used to observe several transitions of the Meinel 1–0 band of N_2^+ with linewidths of $\sim$120 MHz. An optical frequency comb has been used for absolute frequency calibration of transition frequencies to within $\sim$8 MHz. This work represents the first direct spectroscopy of an electronic transition in an ion beam, and also represents a major step toward the development of routine infrared spectroscopy of rotationally cooled molecular ions.

PACS numbers: 41.75.Ak, 42.62.Fi, 33.20.Ea, 42.62.Eh, 82.80.Rt

I. INTRODUCTION

The study of molecular ions is important in a number of fields, including physical chemistry, combustion chemistry, atmospheric chemistry,[1] and astrochemistry.[2,3] Ions are transient and reactive species, so even in plasma discharges, neutral molecules are typically $\sim$6 orders of magnitude more abundant than the ions of interest. Early spectroscopic studies on glow discharges were often hampered by interfering signals from neutral absorbers.[4] The invention of velocity modulation spectroscopy (VMS),[5] which involves using a high voltage AC discharge to modulate the velocity of ions and a lock-in amplifier to isolate the modulated ionic absorption signals from the unmodulated neutral signals, has allowed for the spectroscopic study of scores of molecular ions.[4] However, due to harsh plasma conditions, molecular ions produced in VMS experiments often have high rotational and vibrational temperatures, typically on the order of several hundred Kelvin. For example, CH_3^+ has been studied by the Oka group in a liquid nitrogen cooled discharge cell, where the rotational and vibrational temperatures were reported as 371 and 700 K, respectively.[6]

Until recently,[7] all VMS experiments produced Doppler-limited line widths of $\gtrsim$1 GHz. For small diatomic molecules, the spectra remain relatively simple to assign and line intensities are fairly strong, but larger (e.g., $C_3H_3^+$) or highly fluxional (e.g., CH_5^+) molecular ions are more challenging targets, as each individual transition is weaker due to quantum dilution. Supersonically expanding discharges have been used to spectroscopically study rotationally cold molecular ions, but the reduced rotational temperature comes with the price of lost ion/neutral discrimination. Although concentration modulation can provide some discrimination from background precursors,[8] radicals[9] and excited states of stable neutrals can still congest and complicate the recorded spectrum.

The limitations of current techniques are highlighted by the case of CH_5^+, a molecular ion of considerable interest due to its lack of a classical structure[10] and as the prototypical non-classical carbocation.[11] The only published high-resolution spectrum of CH_5^+ was recorded by the Oka group[12] in a liquid nitrogen-cooled discharge of H_2 and CH_4, and was identified by a process of elimination, by removing the known spectral lines of H_3^+, CH_3^+, $C_2H_3^+$, HCO^+, $HCNH^+$, the Rydberg spectrum of H_2, and strong lines of CH_4 that remained due to a slight asymmetry in the AC plasma. This rich spectrum ($\sim$ 900 lines, due to the fairly high rotational temperature) may still contain some transitions of other ions, and certainly is missing some CH_5^+ transitions due to overlap with CH_4 lines. As a result of the complexity of the spectrum, it remains completely unassigned more than a decade since its publication.

The Nesbitt group has recorded[13] a spectrum of a supersonically expanding H_2:CH_4 plasma, the broad outline of which has been published.[14] Their spectrum ev-

[a)] Present Address: Department of Chemistry, Illinois Wesleyan University, Bloomington, Illinois 61702, USA.

[b)] Author to whom correspondence should be addressed; Electronic mail: bjmccall@illinois.edu; http://bjm.scs.illinois.edu

idently contains many transitions that coincide with Oka's, but also many transitions that do not. Because of the lack of a rigorous ion/neutral discrimination, it is possible that some of these transitions may be due to excited CH_4. They have proposed[13] the use of four-line combination differences to help assign the spectrum, but this effort requires higher precision in the determination of line centers.[15]

The ideal experiment for studying the spectra of complex ions such as CH_5^+ may be a combination of a supersonic expansion ion source with fast ion beam spectroscopy. This approach offers rigorous ion/neutral discrimination (by physically separating ions from neutrals) and reduced Doppler line widths (from kinematic compression), and also allows mass identification of each spectral line (from Doppler splittings).

The only direct ion beam spectrometer (prior to the present work) was developed in the late 1980s in the Saykally group at Berkeley.[16] This instrument was successfully used to measure the mid-IR absorption spectra of HF^+, HN_2^+, HCO^+, H_3O^+ and NH_4^+,[16–18] but was abandoned after a few years, as it did not have sufficient sensitivity to pursue the spectra of larger or fluxional ions at the rotational temperature of uncooled ion sources.

With an eye to applications such as CH_5^+, we have embarked on an effort to construct a second-generation direct ion beam spectrometer, which incorporates a number of technological advances from the past two decades and is also designed to be fed with a continuous supersonic expansion discharge source.[19] As this approach will combine ultra-high sensitivity, rotational cooling, and very high precision line center determination, we refer to it as Sensitive, Cooled, Resolved Ion BEam Spectroscopy (SCRIBES).

This paper describes an important step toward SCRIBES, in the form of a new ion beam instrument that uses a Ti:Sapphire laser (the future pump laser for a mid-IR difference frequency laser) in concert with noise-immune cavity-enhanced optical heterodyne molecular spectroscopy (NICE-OHMS)[20] as a sensitive direct spectroscopic probe of the ion beam. This instrument uses a time-of-flight mass spectrometer (TOF-MS) to provide mass analysis of constituents of the ion beam at spectroscopically relevant beam energies. An optical frequency comb is used to accurately and precisely measure the frequencies of the observed transitions.

The initial proof of concept system studied in this work is the 1–0 band of the $A^2\Pi_u - X^2\Sigma_g^+$ Meinel system of N_2^+, which is an important species in atmospheric aurorae and electrical discharges. Because the line centers of many transitions in this band have already been measured at Doppler-limited resolution,[21] N_2^+ serves as a useful benchmark of the capabilities of our fast ion beam spectrometer.

II. EXPERIMENTAL

A. Overview

Figure 1 shows an overview of the entire experimental setup, which can be divided into two functional groups: i) the ion beam setup, including the ion source, the ion optics and the mass spectrometer; and ii) the spectroscopic setup, consisting of the laser system and signal detection electronics. The two parts of the system interact in the central overlap region, where the laser cavity and the ion beam are superimposed.

In order to minimize vibrations in the spectroscopic setup, the optical components are mounted on a pneumatically stabilized laser table that is mechanically isolated from the ion beam setup. The mirrors of an optical cavity (finesse $\mathcal{F} \sim 450$) are positioned on breadboards that overhang the edge of the laser table and surround the ion beam drift region. Within the optical cavity, the laser is coupled through Brewster windows mounted on the ion beam chamber, and is overlapped with the ion beam within the drift region.

A cold cathode ion source, described in detail in Section II B, is used to produce a beam of N_2^+ at energies ranging from 2-6 kV. After the beam is extracted from the source, it is focused by an Einzel lens and steered by two sets of parallel electrostatic plates into a cylindrical electrostatic double-focusing deflector.[22] When this deflector is biased, the ion beam is turned 90° and focused into the drift tube. When the deflector plates are grounded, the ion beam proceeds straight through a hole in the outer deflector plate and into a Faraday cup that is used to optimize source conditions for maximum ion current, which is generally $\sim$10 μA.

After exiting the deflector chamber, the ion beam proceeds through a 27 cm long drift tube and two metal plates that are spaced 13 cm apart, centered in the drift region. The metal plates are attached to vertical linear manipulators; each plate has three 3-mm diameter apertures that are spaced 1.5 cm vertically and 1 mm horizontally. The apertures are aligned with the laser horizontally by choosing the hole that does not spoil the cavity finesse, and vertically within a hole by fine-tuning the vertical translation of the plates. After the appropriate apertures are centered on the laser, the ion beam is steered through the same apertures to make the laser and the ion beam collinear. The drift tube and the aperture plates are all electrically isolated from the surrounding chamber and connected to one another so they can all be used to modulate the velocity of the ion beam with an applied voltage. After the drift region, the ion beam enters the second 90° bender which guides the ions out of the laser cavity into the time-of-flight mass spectrometer, which is described in detail in Section II D.

Optical spectroscopy of the ion beam is performed using the NICE-OHMS[20] technique, which combines the long effective path length of cavity enhanced spectroscopy with the noise suppression of heterodyne spec-

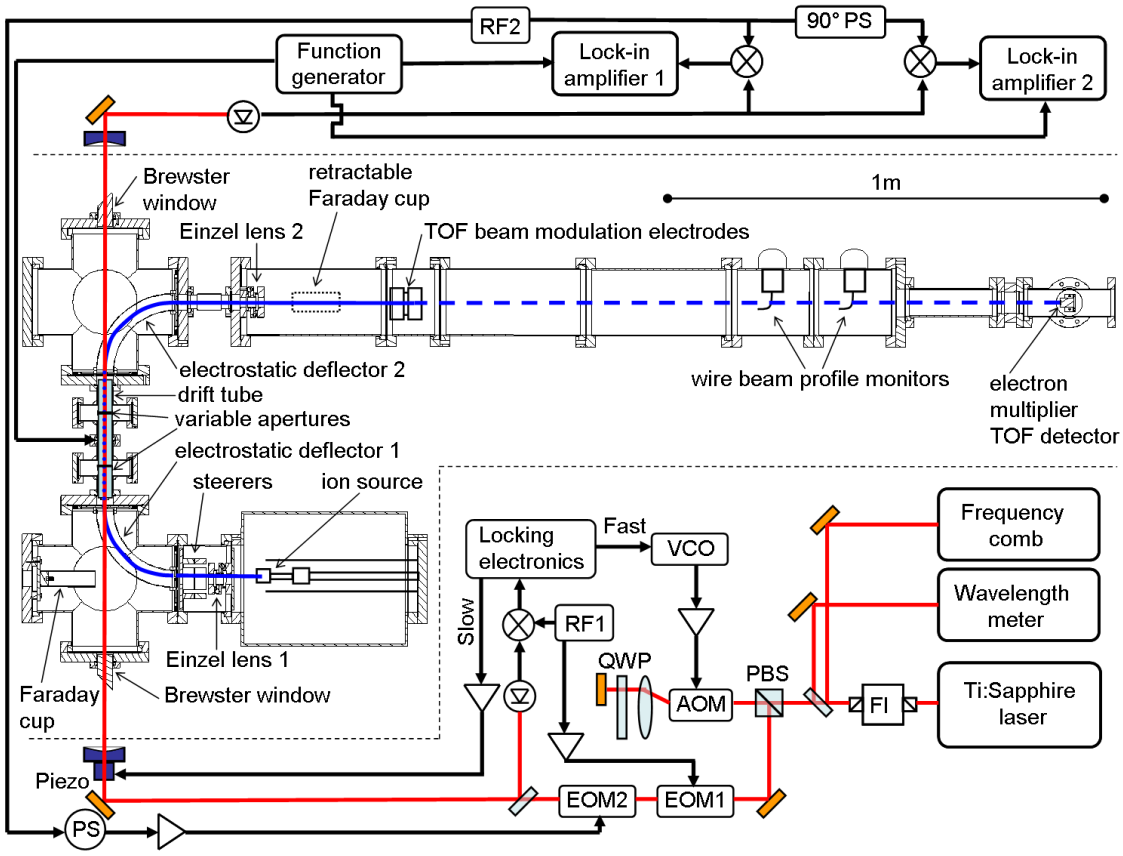

FIG. 1. Color online. Schematic of the fast ion beam spectrometer using NICE-OHMS detection. The following abbreviations are used: Faraday isolator (FI), polarizing beam splitter (PBS), double pass acousto optic modulator (AOM), quarter wave plate (QWP), electro optic modulator (EOM), radio-frequency synthesizer (RF), voltage controlled oscillator (VCO), phase shifter (PS), and time-of-flight (TOF). Amplifiers are indicated with triangles.

troscopy. Further noise suppression is obtained by modulating the velocity of the ions by applying a square wave voltage to the drift tube. A more thorough description of the detection system is given in Section II E.

B. Ion Source

Our instrument is engineered to accommodate a continuous supersonic expansion discharge source, such as the one we have previously characterized for H_3^+ spectroscopy.[19] To utilize such a source, our ion source chamber was designed to be large in size, and to couple to a high-throughput Roots pumping system through large-diameter tubing. However, for the initial testing of the instrument described here, we have designed a modular cold cathode discharge source for simplicity.

Our cold cathode source was made with a fused silica tube held by two electrodes, with an opening at the back for sample gas inlet, and another at the front through which ions are extracted. The electrodes are constructed using stock Ultra-Torr (Swagelok) unions. High temperature silicone O-rings are used to make seals to the fused silica tube which has ground-polished ends. The front electrode uses a custom modified ferrule with a 1 mm diameter aperture to allow ions to be extracted, and a 22° bevel to reduce beam expansion induced by space-charge interaction.[23,24] A small circle of stainless steel mesh was used in the back electrode to produce a more uniform electric field while still allowing gas to flow through the inlet. This source has proven to be robust, operating for typically 40 hours before the front ferrule needs to be cleaned and the fused silica tube interchanged.

A schematic view of the source and its electrical connections is shown in Figure 2. An aluminum cap holds the back electrode to provide mechanical stability and allow for electrical and water-cooling connections. The ions are extracted through a 0.25" diameter hole in a grounded stainless steel plate after the front electrode.

The front electrode (cathode) is biased to 2-6 kV by the "float power supply," which determines the ion beam voltage. The rear electrode (anode) is biased to an additional 3.5 kV above the beam voltage by the "discharge power supply," the ground of which is floated to the beam voltage by the float power supply. The discharge supply is powered through an isolation transformer, and fully enclosed in a polycarbonate box for safety.

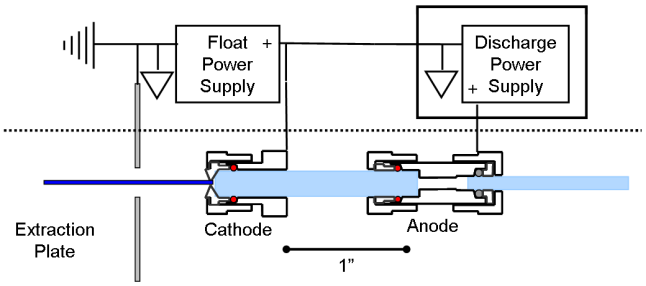

FIG. 2. Color online. A schematic of the cold cathode source and its electrical connections. Gas flows in from the right, and ions are extracted to the left. In this figure, the triangles indicate the “ground” connections of the power supplies; the polycarbonate isolation box for the discharge power supply is also indicated.

C. Ion optical system

The vacuum system, with the exception of the ion source chamber, is made from standard stainless steel Conflat components in order to achieve high vacuum conditions. The homebuilt ion source chamber, which is designed with a high-throughput expansion source in mind, is currently pumped by a 2000 L/s turbomolecular pump and has a pressure of $\sim 5 \times 10^{-6}$ Torr during operation.

The overlap and mass spectrometry regions are pumped by two 500 L/s turbomolecular pumps situated below the 90° deflector chambers, establishing typical pressures during operation of 6×10^{-7} Torr at deflector 1 and 8×10^{-8} Torr at deflector 2. The vacuum cross that houses the mass spectrometer detector is pumped by a 250 L/s turbomolecular pump, and has a typical pressure of $\sim 2 \times 10^{-8}$ Torr.

The ion optical configuration was designed to optimize the ion density in the laser/ion overlap region between the two electrostatic deflectors. All ion optical elements are electrostatic, so all particles with the same kinetic energy and charge state are guided on the same trajectory regardless of particle mass. The positive ions that emerge from the ion source with a voltage V_{beam} are initially focused by the first Einzel lens. In the next short vacuum nipple the ion beam traverses a set of two parallel plate steerers. Each set of steerers can be used to deflect the ion beam both horizontally and vertically, allowing for an adjustment of the beam angle as well as for parallel offsets to the ion beam position. Each steerer plate is supplied by an independent bipolar power supply with voltages up to ± 1000 V. By applying voltages of the same sign to opposing steerer plates, it is also possible to induce additional horizontal or vertical focusing in the steerer section.

The cylindrical 90° deflectors follow a new design[22] that provides control of the ion beam focusing in both dimensions, unlike traditional cylindrical or quadrupole deflectors that create an astigmatic output beam. Our cylindrical deflectors use plates of differing plate heights to mimic the field of a spherical deflector at the ideal ion beam orbit without the cost and size of a true spherical deflector.

In operation, about 50% of the 10 μA ion beam current that is measured in the Faraday cup in the first ion deflector chamber can be transported through the overlap region and both deflectors and collected in the retractable Faraday cup after deflector 2. But once the 3 mm apertures are put into place in the drift region, only 1-2 μA of beam current make it through the system. After traversing the overlap region, the ion beam is turned by the second deflector, collimated by a second Einzel lens, and directed into the time-of-flight mass spectrometer.

D. Time of flight mass spectrometer

1. MS design

The Saykally ion beam instrument used a Wien velocity filter as a mass analyzer to identify the ions present in their beam and to optimize the current of the ion of interest. However, due to the relatively low mass resolution of the Wien filter, this optimization was performed at a lower beam energy than that at which spectroscopy was performed.[16–18]

In contrast, we have adopted a beam modulation[25,26] time-of-flight mass spectrometer (TOF-MS), which creates an ion packet from our continuous ion beam. This technique can perform mass and energy analysis at full beam energy, thereby avoiding the possibility that the ion beam composition may be dependent on the extraction voltage. Figure 1 shows the TOF-MS region, consisting of an Einzel lens and a pair of vertical electrostatic deflector plates. The deflection plates are held at an equal voltage but with opposite polarity. The polarity of the plates is then quickly reversed to sweep the ion beam over a 3.2 mm diameter aperture located near the detector. Two beam profilers aid in aligning the ion beam through the 1.53 m drift tube and onto the electron multiplier detector. At a beam voltage of 4 kV, our TOF-MS has a measured resolution of $m/\Delta m \sim 400$, which will be sufficient for optimizing the production of even large molecular ions such as $C_6H_7^+$.

2. MS results

The mass spectrometer is used to (i) identify the ion species in the plasma, (ii) estimate the beam energy and (iii) calculate the energy spread of the ions created by the cold cathode plasma source. In a nitrogen plasma under typical conditions, the source produces mostly N_2^+ and N^+ in a ratio of 10:1, as shown in Figure 3. The field-free flight tube length combined with arrival times of individual ions can be used to estimate both the average beam energy as well as the energy spread of the ions in the beam, as shown in Figure 3. For a beam

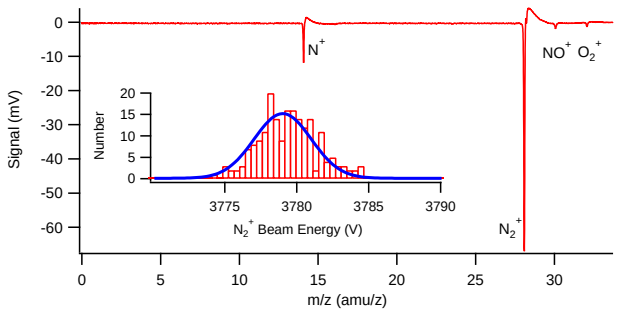

FIG. 3. Mass spectrum of an ion beam formed from a N_2 plasma, showing a N_2^+:N^+ ratio of ∼10:1. The inset shows the energy distribution of the N_2^+ ions.

voltage of ∼3780 V, the energy spread was found to be 4.7 V (FWHM), which is consistent with the spectroscopic linewidths presented in Section III A.

E. Spectroscopy

1. Heterodyne detection

The Ti:sapphire laser, optical cavity, locking scheme,[7,27] and the NICE-OHMS technique[28] have been described previously, so only a brief overview is given here. Two sets of RF sidebands are added by electro optic modulators (EOM). The first non-resonant EOM adds sidebands at ∼30 MHz with a small modulation index. The signal from a back reflection off of the cavity is demodulated with an RF mixer to generate the Pound-Drever-Hall[29] error signal. An analog lockbox splits corrections from the error signal into slow and fast components. The slow corrections are sent to the cavity piezo to alter the cavity length, while the fast corrections are sent to the voltage controlled oscillator (VCO) that drives the acousto optic modulator (AOM) to make small changes in the laser frequency. As shown in Figure 1, the laser is double passed through a 85 MHz resonant AOM, which makes the pointing of the laser beam immune to changes in the AOM frequency[30] and induces a 170 MHz redshift to the laser light. The second EOM, resonant at 113 MHz, adds sidebands at exactly the free spectral range (FSR) of the optical cavity with a modulation index $\beta \sim 0.83$. The laser is coupled into the cavity, and the light transmitted through the cavity is detected with a fast photodiode.

Heterodyne spectroscopy (including NICE-OHMS) is sensitive to both absorption and dispersion signals, which when unsaturated,[31] are related to one another through the Kramers-Kronig relations. Since the two signals appear 90° out of phase with one another with respect to the RF modulation, it is possible to independently observe each signal with phase sensitive detection. To take advantage of this aspect of the spectroscopy, the AC component of the detector signal is amplified, split into two paths, and demodulated with two separate mixers which are set to be 90° out of phase with one another. The overall detection phase is adjusted using an RF phase shifter in the line between the RF generator and the amplifier that drives the 113 MHz EOM. The RF phase shifter is used to set one mixer to record solely the dispersion phase.

2. Modulation scheme and Doppler splittings

Because residual amplitude modulation (RAM) induced by the EOM or external etalons can limit the sensitivity of NICE-OHMS, it is advantageous to use a second form of modulation.[32] In this work, the velocity of the ions is modulated by a square wave voltage at 4 kHz applied to the drift tube and aperture plates. After the heterodyne RF signal is demodulated with the mixers, the velocity modulation signal is demodulated using the lock-in amplifiers.

Because the laser propagates both parallel and anti-parallel to the fast ion beam, each spectral line is both red (−) and blue (+) Doppler shifted away from the rest frequency (ν_0) to

$$\nu_\pm = \nu_0 \sqrt{\frac{1 \pm v/c}{1 \mp v/c}} \tag{1}$$

where the velocity of the ions $v = \sqrt{2qV'/M}$, q is the charge of an electron, V' is the voltage of the ion beam in the drift tube, and M is the mass of the species. The voltage of the ion beam in the drift tube V' is determined from the modulation voltage (V_{mod}) by $V' = V_{beam} \pm V_{mod}$. (Note that the typical approximation $\nu_\pm \sim \nu_0(1 \pm v/c)$ is inaccurate by ∼ 50 MHz at this frequency.) In a case where multiple ions are present, this Doppler splitting will provide mass-identification of every spectral line.

For example, the red and blue components of a 1.985 kV ion beam of N_2^+ are separated by ∼254 GHz (∼8.47 cm^{-1}). With a 2 V_{pp} square wave driving the velocity modulation, the red and blue components are Doppler split again into components separated by 128 MHz. This splitting is not resolved, given the residual Doppler linewidth (observed to be 90 MHz for the ∼ 2 kV beam) and the 113 MHz sideband spacing.

3. Frequency comb calibration

For ultra-high accuracy and precision on the frequency measurements, an erbium doped fiber amplifier frequency comb (MenloSystems FC1500/0060) is used to precisely calibrate the frequency of our Ti:Sapphire laser. For each point in our spectrum, the frequency of the Ti:Sapphire laser is determined by measuring the beat frequency between the Ti:Sapphire laser and the nearest comb mode.[27,28] In order to demonstrate the precision of the

spectroscopic measurements, several frequency comb calibrated scans are shown in Section III A. The line center for the red Doppler shifted (ν_-) and the blue Doppler shifted (ν_+) components are measured by averaging scans of each component taken with both increasing and decreasing laser frequency, in order to compensate for apparent frequency shifts caused by the finite time constant of the lock-in amplifier. (Our scanning rate corresponds to only ∼12 time constants from the minimum to the maximum of the dispersion profile, whereas a wait time of 10 time constants would be needed for the lock-in to reach 99% of its final value at the presently used 24 dB/octave roll-off.) As can be seen from equation (1), the rest frequency can then be determined as the geometric mean of the frequencies of the red and blue shifted components, $\nu_0 = \sqrt{\nu_-\nu_+}$.

III. RESULTS

A. Spectroscopic results

Two typical scans of the $Q_{22}(14.5)$ line of the 1-0 band of the $A^2\Pi_u - X^2\Sigma_g^+$ Meinel system of N_2^+ are shown in Figure 4. Only the dispersion phase is displayed, because no signal was observed at the absorption detection phase due to optical saturation, as described below.

The line shape function for a dispersion signal for NICE-OHMS is given by[32]

$$\chi_{n-o}^{disp}(\nu_d) = \chi^{disp}(\nu_d - \nu_{fm}) - 2\chi^{disp}(\nu_d) + \chi^{disp}(\nu_d + \nu_{fm}) \quad (2)$$

where χ^{disp} is the general dispersion line shape function, ν_d is the de-tuning ($\nu_d = \nu - \nu_0$) of the carrier from the center frequency (ν_0) of the transition, and ν_{fm} is the RF modulation frequency (113 MHz).

The velocity modulation induces a second Doppler splitting (ν_{vm}) where the positive and negative splitting are 180 degrees out of phase with one another. Therefore, the line shape for a dispersion signal for a NICE-OHMS velocity modulated ion beam signal is

$$\chi_{vm}^{disp} = \chi_{n-o}^{disp}(\nu_d - \nu_{vm}) - \chi_{n-o}^{disp}(\nu_d + \nu_{vm}) \quad (3)$$

The Gaussian dispersion line shape, derived from a peak-normalized Gaussian line shape, is given by[31,33]

$$\chi^{disp}(\nu) = -\frac{2}{\sqrt{\pi}} e^{-\gamma^2} \int_0^{\gamma} e^{\gamma'^2} d\gamma' \quad (4)$$

where $\gamma = 2\nu_d\sqrt{\ln 2}/\Delta\nu$ and $\Delta\nu$ is the full width at half maximum (FWHM) for the Gaussian profile.

When the spectra are fit to Equation 3, the line center, FWHM, and peak-normalized Gaussian amplitude are obtained. An example of the red- and blue-shifted components of a NICE-OHMS signal are shown in Figure 4. The average linewidth for a 4 kV beam was ∼120 MHz, which is consistent with the beam energy spread observed with the TOF-MS. Some slight asymmetry is seen between the amplitudes of the positive and negative velocity modulation components, and appears to be dependent on the alignment and overlap of the ion beam with the laser beam, which we have not yet fully optimized. We expect to have more useful diagnostic information regarding this asymmetry when we move to mid-infrared spectroscopy, as the narrower linewidth will enable a full resolution of the heterodyne and velocity modulation splittings.

Figure 5 shows an example of how spectra calibrated with the frequency comb are used to determine the line center. For each red- and blue-shifted component of the NICE-OHMS signal, scans in opposite directions were collected, as described above. The average of the blue-shifted transitions was $\nu_+ = 10865.19163$ cm^{-1} and the average of the red-shifted transitions was found to be $\nu_- = 10853.49936$ cm^{-1}. The geometric mean of these two values gives a rest transition frequency of $\nu_0 = 10859.34392$ cm^{-1}, which is within 8 MHz of the rest frequency of 10859.34418 cm^{-1} measured with sub-Doppler resolution and frequency comb calibration in a positive column discharge.[28] This accuracy appears to be limited primarily by the asymmetry in the observed lineshapes (the optical frequency comb itself has an accuracy $\ll 1$ MHz), and so we expect this to be further improved in the future.

B. Sensitivity and Saturation

For a baseline scan obtained with a 3 s lock-in time constant (and a 24 dB/octave roll-off, with a resulting detection bandwidth of 0.03 Hz), the observed noise equivalent absorption is $\sim 2\times10^{-11}$ cm^{-1} Hz$^{-1/2}$, which is a factor of 50 lower than the Saykally ion beam instrument.[16] The improvement comes from several factors: a lower fractional noise level at the detector (1.3×10^{-8} vs. 2×10^{-7}), thanks in part to heterodyne detection; a higher cavity finesse ($\mathcal{F}$, 450 vs. 100); and a longer laser/ion overlap length (L, 27 cm vs. 15 cm).

The shot noise limit for the instrument is given by[34]

$$\sigma_{\text{shot noise}} = \frac{\pi}{\mathcal{F}\times L}\sqrt{\frac{qB}{\eta P_0}}\frac{1}{J_0(\beta)J_1(\beta)} \quad (5)$$

where q is the charge of an electron, B is the bandwidth of detection, η is the detector responsivity, P_0 is the power incident on the detector, and $J_n(\beta)$ are Bessel functions of the heterodyne modulation index, β. The effective path length through the ion beam is the laser/ion beam interaction length (L=27 cm) times the number of round trip passes ($\mathcal{F}/\pi$). At a typical power level (incident on the detector) of 1.10 mW, the expected fractional shot noise is $\sim 2\times10^{-12}$ cm^{-1}. Thus, the observed noise in the instrument ($\sim 3\times10^{-12}$ cm^{-1}) is within a factor of ~ 1.5 of the shot noise limit.

Absorption signals are not observable in this experiment due to the high degree of optical saturation, which

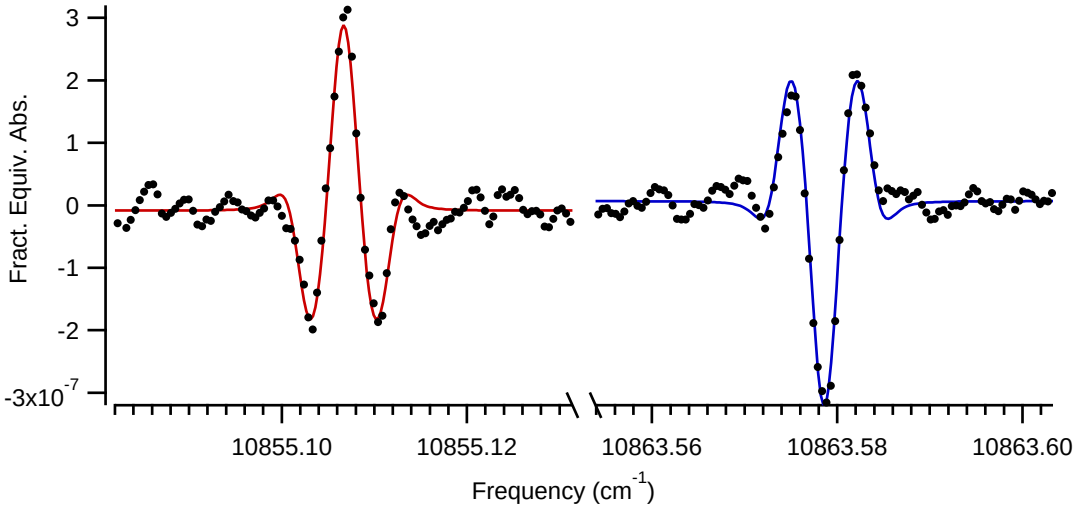

FIG. 4. Color online. Scans of red- and blue-shifted components of the $Q_{22}(14.5)$ line (black dots) collected at 1.985 kV beam voltage along with fits to Equation 3 (solid curves). For clarity, only 1 in every 15 experimental points is shown. The Doppler shifted lines are 180° out of phase with one another, allowing for identification of the sign of a component's Doppler shift. The Doppler shifted components are separated by $\sim$8.5 cm^{-1} as expected from Equation 1.

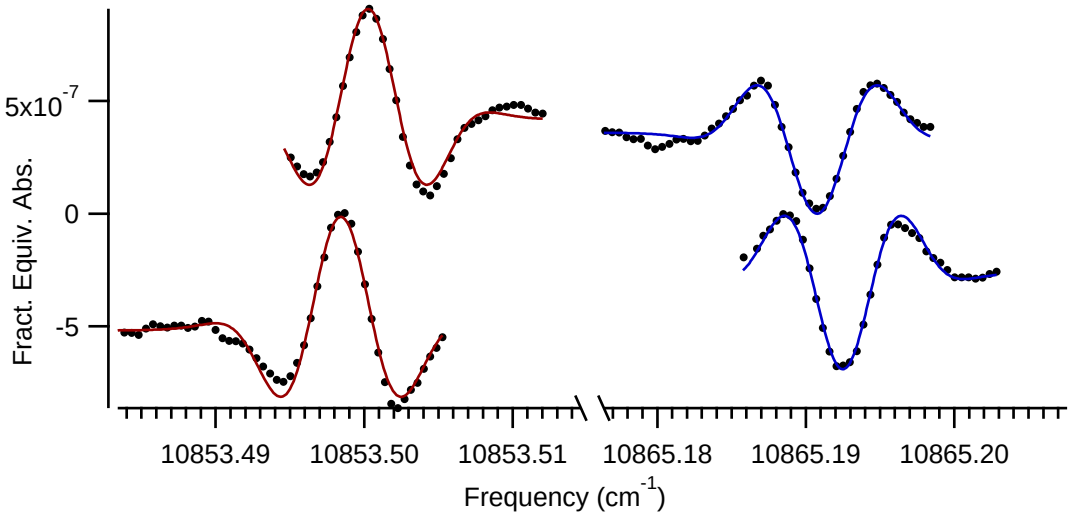

FIG. 5. Color online. Scans of red- and blue-shifted components of the $Q_{22}(14.5)$ line (black dots) collected at 3.781 kV beam voltage along with fits to Equation 3 (solid curves) where the frequency axis is calibrated with the frequency comb. For clarity, only 1 in every 15 experimental points is shown. The top two traces are scanned toward the rest frequency and the bottom are scanned away from the rest frequency. As discussed in the text, the apparent frequency shifts are artifacts of the lock-in detection. The spectra have been offset vertically for clarity.

is due to the high intracavity laser power and the lack of any relaxation process for the ions in the beam. For typical experimental conditions, we estimate the saturation parameter[31] of G_0 $\sim$30,000 for the carrier and G_1 $\sim$6,300 for the sidebands. The absorption signal should be reduced by a factor of $\sqrt{1+G_1}$ $\sim$80, and is not detectable given our signal-to-noise ratio.

The impact of saturation on the dispersion signal in NICE-OHMS is strongly dependent on the ratio between the homogenous linewidth in the absence of saturation and the Doppler width (this ratio is denoted y in ref. 31). Assuming the homogenous linewidth is set by the transit time ($\sim$1.6 μs for a 4 kV beam), and that the Doppler width is 120 MHz (from our fits), we expect y $\sim$0.0038, and the dispersion signal should be reduced by only a factor of $\sim$ 2 at these saturation parameters.

However, the observed dispersion signals are a factor of $\sim$14 weaker than would be expected based on the ion number density and the transition strength. At present, we can only speculate as to the reason for this discrep-

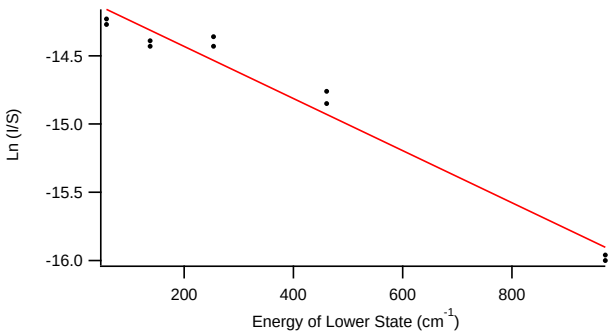

FIG. 6. Boltzmann diagram for observed N_2^+ transitions; for each transition, a separate measurement is shown for each of the red- and blue-shifted components to illustrate the reproducibility of the intensities. The calculated rotational temperature is 753±45 K.

ancy; possible reasons include: (1) not all N_2^+ ions may be in the vibronic ground state, (2) the actual Doppler-width may be narrower than the observed width if the latter has contributions from jitter in the beam energy caused by the power supplies, and (3) the overlap between the ion beam and the laser beam may be imperfect [as suggested by the asymmetries in the lines]. We anticipate that future experiments in the mid-infrared will shed further light on this discrepancy.

C. Discussion

In order to characterize the rotational distribution of the N_2^+ ions produced by our ion source, spectra of the ${}^qQ_{22}(J)$ lines (with J=4.5, 7.5, 10.5, 14.5 and 21.5) with lower energies ranging from 60 to 970 cm^{-1} were collected. The spectra were fit to Equation 3. The observed intensities (I) were normalized to the strength (S) of the transition, which was obtained along with the lower state energies from PGopher[35] using constants from Reference 21. Figure 6 shows a Boltzmann diagram for the five observed transitions. From the slope of the linear regression fit, the rotational temperature is 753±45 K.

While we only observed several transitions, this highly resolved technique could easily be applied to the observation of tens or hundreds of transitions. As the previous work[21] observed Doppler-limited transitions with linewidths of 1-1.4 GHz, the line centers were only determined to a precision around 60 MHz, with an accuracy of 150 MHz. With modest improvements to our current system, the accuracy of line center determination could be improved by at least a factor of 50 compared to the Doppler-limited measurements. This would greatly improve the overall RMS of the current effective Hamiltonian fit (RMS ∼ 100 MHz) and the individual observed–calculated values for many blended lines.

Finally, it should be noted that ion beam spectra enjoy a completely rigorous ion/neutral discrimination, both from the spatial separation of the ions from the neutrals and from the velocity modulation. While our previous cavity-enhanced velocity modulation technique studies[7,27,28] showed a discrimination between ions and neutrals in the lock-in detection phase, the ion beam technique is rigorously insensitive to absorbing or dispersing neutrals.

IV. CONCLUSIONS AND FUTURE DIRECTIONS

We have demonstrated the construction of a fast ion beam spectrometer which provides rigorous spatial and velocity modulation discrimination against neutral signals. We have demonstrated the instrument's capabilities by showing narrow (∼ 120 MHz) spectral lines from the $A^2\Pi_u - X^2\Sigma_g^+$ system of N_2^+; this represents the first direct spectroscopy of an electronic transition in an ion beam. The ion beam instrument has a high-resolution mass spectrometer that provides online mass spectra at spectroscopically relevant beam energies. The dispersion line shape of the NICE-OHMS signal has been described, as well as the sensitivity and the observed noise. With the current detectors and laser power, the noise is close to the shot noise limit. The NICE-OHMS instrument reported in this article has been shown to be a factor of 50 more sensitive than the previous direct absorption ion beam instrument.[16] The rotational temperature of ions in the ion beam was found to be ∼750 K.

The laser spectroscopy reported here was based on using two EOMs on a frequency tunable Ti:Sapphire laser. By combining the output of this Ti:Sapphire with a cw Nd:YAG laser in a periodically-poled lithium niobate crystal, a mid-IR laser with appropriate sidebands can be generated. This will enable the extension of this NICE-OHMS ion beam spectroscopy technique into the mid-IR to record the fundamental vibrational bands of a wide variety of molecular ions in the 2.8–4.8 μm region.

Finally, it is expected that a continuous supersonic expansion discharge source[19] and skimmer will replace the cold cathode ion source in the near future. The use of a supersonic expansion will enable the spectroscopy of larger and more fluxional molecular ions (e.g., CH_5^+ and $C_3H_3^+$), for which quantum dilution at higher rotational temperatures has complicated previous attempts to apply velocity modulation spectroscopy.

ACKNOWLEDGMENTS

The design, construction, and commissioning of this ion beam spectrometer involved substantial contributions from a number of current and previous members of our group. In particular, we wish to thank Susanna Widicus Weaver, Matthew Zwier, Jeffrey Carter, and Kyle Ford. This work would not have been possible without the skilled craftsmanship of the School of Chemical Sciences Machine Shop and Electronics Shops. The authors

also wish to acknowledge helpful conversations regarding ion beam spectrometer design with Jim Coe and Rich Saykally.

This work has been supported by an NSF CAREER award (CHE 04-49592), an Air Force Young Investigator award (FA9550-07-1-0128), the NASA Laboratory Astrophysics program (NNX08AN82G and NNG05GE59G), a David and Lucile Packard Fellowship, a Camille and Henry Dreyfus New Faculty award, and the University of Illinois. MWP has been supported by a Robert C. and Carolyn J. Springborn Fellowship from the University of Illinois.

[1] E. E. Ferguson, F. Arnold, Acc. Chem. Res. 14 (1981) 327–334.
[2] E. Herbst, W. Klemperer, Ap. J. 185 (1973) 505–533.
[3] T. Oka, M.-F. Jagod, J. Chem. Soc., Faraday Trans. 89 (1993) 2147–2154.
[4] S. K. Stephenson, R. J. Saykally, Chem. Rev. 105 (2005) 3220–3234.
[5] C. S. Gudeman, M. H. Begemann, J. Pfaff, R. J. Saykally, Phys. Rev. Lett. 50 (1983) 727–731.
[6] M. F. Jagod, C. M. Gabrys, M. Rosslein, D. Uy, T. Oka, Can. J. Phys. 72 (1994) 1192–1199.
[7] B. M. Siller, A. A. Mills, B. J. McCall, Opt. Lett. 35 (2010) 1266–1268.
[8] S. Davis, M. Farnik, D. Uy, D. J. Nesbitt, Chem. Phys. Lett. 344 (2001) 23–30.
[9] D. T. Anderson, S. Davis, T. S. Zwier, D. J. Nesbitt, Chem. Phys. Lett. 258 (1996) 207–212.
[10] K. C. Thompson, D. L. Crittenden, M. J. T. Jordan, JACS 127 (2005) 4954–4958.
[11] G. A. Olah, G. Klopman, R. H. Schlosberg, JACS 91 (1969) 3261.
[12] E. T. White, J. Tang, T. Oka, Science 284 (1999) 135–137.
[13] C. Savage, F. Dong, D. J. Nesbitt, presentation at 61st International Symposium on Molecular Spectroscopy, Columbus, OH, 19-23 June (2006).
[14] X. Huang, A. B. McCoy, J. M. Bowman, L. M. Johnson, C. Savage, F. Dong, D. J. Nesbitt, Science 311 (2006) 60–63.
[15] D. J. Nesbitt, presentation at the 8th International Conference of Computational Methods in Sciences and Engineering, Kos, Greece, 3 October (2010).
[16] J. V. Coe, J. C. Owrutsky, E. R. Keim, N. V. Agman, D. C. Hovde, R. J. Saykally, J. Chem. Phys. 90 (1989) 3893–3902.
[17] J. C. Owrutsky, E. R. Keim, J. V. Coe, R. J. Saykally, J. Phys. Chem. 93 (1989) 5960–5963.
[18] E. R. Keim, M. L. Polak, J. C. Owrutsky, J. V. Coe, R. J. Saykally, J. Chem. Phys. 93 (1990) 3111–3119.
[19] K. N. Crabtree, C. A. Kauffman, B. J. McCall, Rev. Sci. Instrum. 81 (2010) 086103.
[20] J. Ye, L. S. Ma, J. L. Hall, J. Opt. Soc. Am. B 15 (1998) 6–15.
[21] D. W. Ferguson, K. N. Rao, P. A. Martin, G. Guelachvili, J. Mol. Spectrosc. 153 (1992) 599–609.
[22] H. Kreckel, H. Bruhns, K. A. Miller, E. Wahlin, A. Davis, S. Hockh, D. W. Savin, Rev. Sci. Instrum. 81 (2010) 063304.
[23] J. H. Moore, C. C. Davis, M. A. Coplan, Building Scientific Apparatus, Perseus Books, 2002.
[24] J. R. Pierce, J. Appl. Phys. 11 (1940) 548–554.
[25] J. M. B. Bakker, J. Phys. E 6 (1973) 785–789.
[26] J. M. B. Bakker, J. Phys. E 7 (1974) 364–368.
[27] A. A. Mills, B. M. Siller, B. J. McCall, Chem. Phys. Lett. 501 (2010) 1 – 5.
[28] B. M. Siller, A. A. Mills, M. Porambo, B. J. McCall, Opt. Express Accepted (2011).
[29] R. W. P. Drever, J. L. Hall, F. V. Kowalski, J. Hough, G. M. Ford, A. J. Munley, H. Ward, Appl. Phys. B 31 (1983) 97–105.
[30] E. A. Donley, T. P. Heavner, F. Levi, M. O. Tataw, S. R. Jefferts, Rev. Sci. Instrum. 76 (2005) 063112.
[31] W. Ma, A. Foltynowicz, O. Axner, J. Opt. Soc. Am. B 25 (2008) 1144–1155.
[32] A. Foltynowicz, F. M. Schmidt, W. Ma, O. Axner, Appl. Phys. B 92 (2008) 313–326.
[33] A. Foltynowicz, W. G. Ma, F. M. Schmidt, O. Axner, J. Opt. Soc. Am. B 25 (2008) 1156–1165.
[34] J. Ye, Ultrasensitive high resolution laser spectroscopy and its application to optical frequency standards, Dissertation, University of Colorado Department of Physics, 1997.
[35] C. M. Western, Pgopher, a program for simulating rotational structure, http://pgopher.chm.bris.ac.uk, 2009.